Lehrstuhl für Raumfahrttechnik
Prof. Dr. rer. nat.
Ulrich Walter

Otto-von-Taube-Gymnasium

Seminararbeit

Development and Integration of a Sun Sensor for the Pico-Satellite MOVE

Author:

Dominik von Mengden

Supervision: Dipl.-Ing. Claas Olthoff
Lehrstuhl für Raumfahrttechnik / Institute of Astronautics
Technische Universität München

Stefan Mahnke
Otto-von-Taube-Gymnasium Gauting

Erklärung

Ich erkläre, dass ich alle Einrichtungen, Anlagen, Geräte und Programme, die mir im Rahmen meiner Semester- oder Diplomarbeit von der TU München bzw. vom Lehrstuhl für Raumfahrttechnik zur Verfügung gestellt werden, entsprechend dem vorgesehenen Zweck, den gültigen Richtlinien, Benutzerordnungen oder Gebrauchsanleitungen und soweit nötig erst nach erfolgter Einweisung und mit aller Sorgfalt benutze. Insbesondere werde ich Programme ohne besondere Anweisung durch den Betreuer weder kopieren noch für andere als für meine Tätigkeit am Lehrstuhl vorgesehene Zwecke verwenden.

Mir als vertraulich genannte Informationen, Unterlagen und Erkenntnisse werde ich weder während noch nach meiner Tätigkeit am Lehrstuhl an Dritte weitergeben.

Ich erkläre mich außerdem damit einverstanden, dass meine Diplom- oder Semesterarbeit vom Lehrstuhl auf Anfrage fachlich interessierten Personen, auch über eine Bibliothek, zugänglich gemacht wird, und dass darin enthaltene Ergebnisse sowie dabei entstandene Entwicklungen und Programme vom Lehrstuhl für Raumfahrttechnik uneingeschränkt genutzt werden dürfen. (Rechte an evtl. entstehenden Programmen und Erfindungen müssen im Vorfeld geklärt werden.)

Ich erkläre außerdem, dass ich diese Arbeit ohne fremde Hilfe angefertigt und nur die in dem Literaturverzeichnis angeführten Quellen und Hilfsmittel benutzt habe.

Garching, den _____

_____
Unterschrift

Name: Dominik von Mengden

Acknowledgement

I would like to thank Prof. Dr. Ulrich Walter and the entire staff at the Institute of Astronautics (TUM) for giving me the opportunity to conduct this project in corporation with the Otto-von-Taube-Gymnasium Gauting. Very special thanks go to Claas Olthoff for supervising this project and for his dedication, support, and expert advises. For technical advice and assistance I would also like to thank Tobias Abstreiter, Leonhard Röpfl, and Lars Schelde.

In addition I thank my supportive teachers at school; especially Dr. Magdalena Kaden and Stefan Mahnke, for helping me out whenever the necessity arose.

Zusammenfassung

Das Ziel dieses Projektes war es, einen Prototypen eines Nachfolgesensors für den Nanosatelliten MOVE zu entwickeln, der die relative Lage des 10 x 10 x 10 cm kleinen Satelliten im Weltraum bestimmen kann.

Teil der Studie war eine ausführliche Analyse des Standes der Technik bezüglich heutiger Sensorenmodelle, die Entwicklung eines Sonnensensors und dessen Verifizierung zusammen mit dem bestehenden Sonnensensor des Satelliten und einer Triple-Junction-Solarzelle. Für diesen Zweck wurde im Verlauf der Arbeit ein Teststand entworfen, der verschiedene Lagemöglichkeiten des Satelliten relativ zu einer Lichtquelle mit Hilfe eines Zwei-Achsen Motors in einer weltraumähnlichen Umgebung simuliert.

Alle drei Systeme wurden unter gleichen Testbedingungen auf ihre durchschnittliche Messabweichung überprüft, um sie einheitlich vergleichen zu können. Das Testergebnis der Solarzelle basierte auf geglätteten Werten (wegen starkem Rauschen in der Messschaltung) und ergab eine Abweichung von 2,3° innerhalb eines Sichtfeldes von 90°. Im selben Sichtfeld zog der Test des bestehenden Sensors eine Abweichung von 6,9° nach sich, während das neu entwickelte System eine Messabweichung von nur 1,08° erzielte.

Aus den Ergebnissen ist deutlich zu erkennen, dass der in diesem Projekt entwickelte Sensor in Hinblick auf seine Genauigkeit das geeignetste der drei Systeme für den Satelliten ist. Nachdem sich diese Arbeit auf die Entwicklung und Verifizierung eines Sensorprototypen beschränkt, werden im Laufe der Arbeit außerdem neu entstandene Aufgabenfelder hinsichtlich der Integration des Sensors präsentiert.

Abstract

The purpose of this project was to develop a sensor prototype for an attitude determination system of the pico-satellite MOVE that is capable of identifying the exact orientation of the 10 x 10 x 10 cm satellite in space.

The design of the study involved an elaborate review of state of the art sensor types, the development of a Sun sensor, and the testing of three Sun sensor systems including a triple junction solar cell, an existing and the newly developed sensor model. To fulfill these tasks a test setup was designed using a two axis motor system, which simulates satellite positions relative to a light source in a space-like environment.

All three tested models were verified regarding their orientation determination accuracy, which is expressed in the average measurement error. The flattened values (to compensate for noise in the measurement circuitry) of the solar cell's output achieved an error of 2.3° within a field of view of 90°. In the same range the existing Sun sensor for MOVE yielded an error of 6.9°, while the newly developed system accomplished a measurement error of only 1.08°.

The results showed that the developed Sun sensor qualifies best out of the three systems for future use on the satellite. Since this project focused on the prototype of the sensor, new scopes of future work before final integration and important considerations are also introduced in this paper.

Table of Contents

Index of Figures

Index of Tables

List of Abbreviations

ADS	Attitude Determination System
CAD	Computer-aided Design
CLK	Serial Clock
CPU	Central Processing Unit
CS	Chip Select
DIN	Serial Data In
DOUT	Serial Data Out
DTU	University of Denmark
ECI	Earth-centered inertial coordinate system
FOV	Field of View
GND	Ground
GPS	Global Positioning System
Gyro	Gyroscope
IGRF	International Geomagnetic Reference Field
IMU	Inertial Measurement Unit
IRU	Inertial Reference Unit
LEO	Low-Earth orbit
LGCV	Local Geocentric Vertical coordinate system
LISA	Lightweight Intersatellite-Antenna
LRT	Lehrstuhl für Raumfahrttechnik / Institute of Astronautics
MOVE	Munich Orbital Verification Experiment
PCB	Printed Circuit Board
PCI	Peripheral Component Interconnect
PSD	Position Sensitive Detector
PXI	PCI Extensions for Instrumentation
SPI	Serial Peripheral Interface Bus
TUM	Technische Universität München / Technical University of Munich

1 Introduction

1.1 The MOVE Project

MOVE (Munich Orbital Verification Experiment) is a pico-satellite project hosted by the Institute of Astronautics at the Technical University of Munich (TUM). It was started in 2006 with the objective to let the students at the TUM gain experience with small-scale satellite missions and to be able to test newly developed payloads in the future. The small satellites, which are developed and constructed at the institute, will be sent to space via "piggyback" (secondary payload) on large rockets. It is therefore important to construct the small orbiter according to the "CubeSat Standard", which is a standard for pico-satellites that limits the size and weight of the satellite to 10 x 10 x 10 cm and 1 kg [1]. Figure 1-1 shows a computer animation of the MOVE satellite.

Figure 1–1: Computer animation of the MOVE satellite

At the same time the set size and weight of the satellite being constructed, has become one of the biggest challenges, because it makes it necessary for every instrument and payload on board the satellite to be as small and light as possible.

The structure and mechanisms of the MOVE satellite have already been manufactured and the institute is currently working on the remaining hardware to be integrated. The launch of the MOVE satellite is estimated for the fourth quarter of 2012.

The following sections introduce the state of the art of attitude determination systems (ADS), which are used to determine a satellite's orientation in space.

1.2 Attitude Determination Systems: State of the Art

Since one of the objectives of the CubeSat constructed by the LRT is to fly scientific and technical payloads, it is often important to know the spacecraft's attitude. The goal of an attitude determination system (ADS) is to determine the orientation (or attitude) of a spacecraft relative to a known reference [2]. Figure 1-2 shows a satellite in orbit around the Earth with its known body-fixed frame.
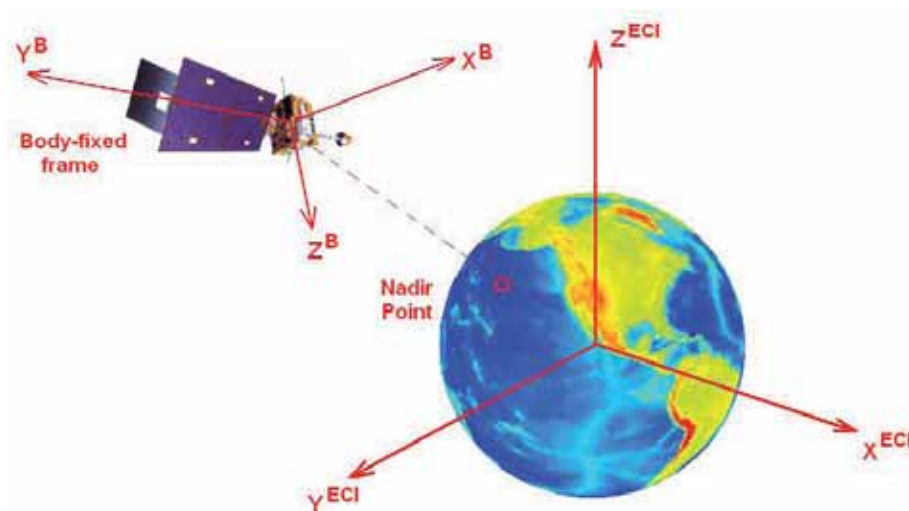
Figure 1–2: A satellite's body-fixed frame and the Earth's known reference frame [2]

An ADS is capable of determining the orientation of a satellite's body-fixed frame with respect to an external reference frame. This can be done, for example, by using the sun, the local magnetic field direction or the stars as a reference. Each external reference (e.g. a measured vector pointing in the direction of the sun) provides only two of the three needed independent parameters (angular distance of the body-fixed frame axes to the measured vector) to specify the spacecraft's attitude [3] (page 355). Like in figure 1-3, for a spacecraft in Earth orbit this can be done by the determination of the local geocentric vertical coordinate system (LGCV), of which the z-axis is the nadir, while the x- and y- axes are vectors pointing in the geographic directions (North, South, East and West) of the geodetic datum (reference on Earth [4]) [5]. The nadir is the downward-facing viewing geometry of the orbiting satellite and is equal to the vertical direction that points in the direction of the force of gravity [6]. This again is equal to the centripetal force of the satellite and therefore points in the direction of the origin of the Earth's frame. The abbreviation ECI in the coordinate system (figure 1-2)

stands for the use of the Earth-centered inertial coordinate system, which has its origin in the geocenter [5]. Figure 1-3 shows the same satellite as in figure 1-2, but with the LGCV reference coordinate system determined and computed by an ADS [2].
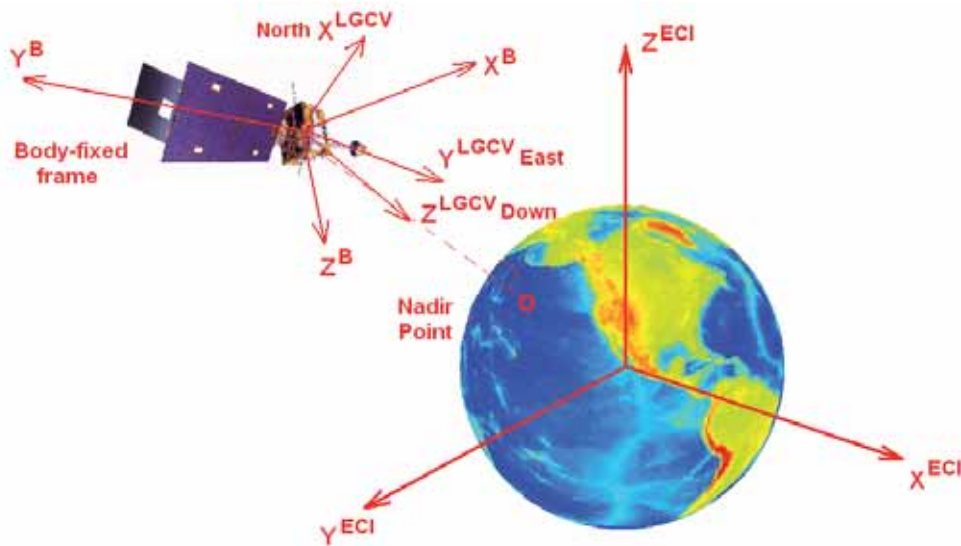
Figure 1–3: The satellite's LGCV coordinate system determined by an ADS [2]

The two frames (body-fixed frame and LGCV) enable the ADS to compute the satellite's orientation with respect to the determined reference frame (LGCV). One way to compute the difference in orientation between the two frames is to calculate yaw, pitch and roll of the satellite relative to the reference frame. These are the angles of rotation in three dimensions about the spacecraft's center of mass [7] (page 334). Figure 1-4 depicts this method. The red frames are body-fixed and the black frames are the LGCV reference frames.
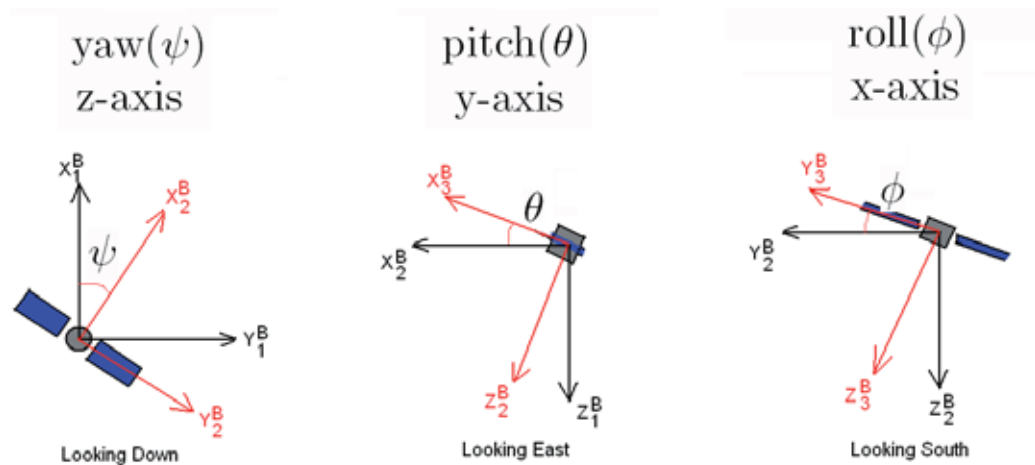
Figure 1–4: Yaw, pitch and roll angles of the satellite [2]

The purpose of an ADS can vary depending on the satellite mission. The most common purposes are navigation feedback for satellites with active attitude control (change of torque using actuators) and attitude information for the pointing of communication antennas [2]. For remote sensing of the Earth's atmosphere or surface, for example, it is very useful to know the nadir of a satellite.

Active attitude control is especially important for satellites with a long lifespan. A space vehicle is always subject to disturbance torques in space, as a result of gravity-gradient effects, magnetic field torques, impingement by solar radiation, and, depending on altitude, aerodynamic torques [3] (page 364). It can experience two kinds of different disturbance torques: cyclic or secular. Cyclic torques vary as a sinus function during an orbit, while secular torques accumulate with time and do not average out over an orbit. Although these disturbances are mostly only in the range of around $10^{-4}Nm$, they can over time cause the spacecraft to be reoriented. To prevent this from happening most spacecraft use either magnetic property to passively stabilize along the magnetic field or sense the disturbances using an ADS to actively apply corrective torques [3] (page 354).

To determine the reference coordinate system of a spacecraft the ADS fuses data from several different subsystems (sensors). The following sections are concerned with the most common types of attitude determining sensors used for spacecraft. Generally, the sensors are divided into two groups, the inertial- and the angle (or vector) sensors [2].

1.2.1 Inertial Sensors

Inertial (or rate) sensors determine the rate of rotation of the satellite in space. Two types of inertial sensors will be introduced in the following sub-sections.

1.2.1.1 Gyroscopes

Gyroscopes (gyros) measure the speed or angle of rotation (rotation rate) around various spacecraft axes with respect to an initial reference. No external reference frame is used to accomplish attitude determination. Today different kinds of gyros are available where the models range from simple spinning wheels, including iron gyros using ball or gas bearings, to more accurate ring laser gyros. A non-laser gyro may also be suspended using a set of gimbals, where the change in gimbal angles is measured to determine the attitude-rate. This is based on the fact that the angular momentum vector of a spinning body is constant in space [7] (page 371). Due to the fact that gyros do not have an external reference (like the LGCV frame), they lack the ability to provide absolute orientation information. One individual gyro can provide one to two axes of information. To provide rotational rate information for all three axes, several gyros are commonly grouped together into inertial reference units (IRU). To finally obtain the spacecraft's rotational position with respect to the initial reference the measured rates have to be integrated over a period of time [7] (page 371). The concept of a gyroscope enables very high bandwidth and extremely sensitive attitude-rate information. As stated earlier though, they can only rely on one initial reference frame, which naturally results in systematic errors in attitude determination over time due to the effects of drift and inaccuracies of integration. These effects are also caused by the mechanics of a gyro rotor, which cannot be maintained in truly torque-free motion [7] (page 371). For this reason, it is common to add other sensors (as the ones listed in section 1.2.2) to make up for the attitude determination errors by recalibrating the gyro periodically. Models of high accuracy are mostly heavy and rather expensive [7] (page 371). Figure 1-5 depicts one of NASA's Gravity Probe B gyroscopes, which is an ultra-precise gyro used to measure Albert Einstein's hypothesized geodetic effect [8]. It also shows a commercial ring-laser gyro, which measures differences in laser interference patterns to determine rotation rates [2].

Figure 1–5: NASA's Gravity Probe B gyro (coated gyro rotor and its housing) (left) [8] and commercial ring laser gyro (right) [2]

1.2.1.2 Accelerometers

Accelerometers are used to determine the time rate of change of velocity of a spacecraft. This is defined as the acceleration of the space vehicle [9]. There are several different categories of acceleration sensors. An example is the use of the piezoelectric effect, where microscopic crystal structures output a voltage relative to their acceleration due to structural stress caused by the accelerative forces. Other systems make use of the Hall effect by sensing the change in magnetic fields when accelerated [9].

When an accelerometer is added to an inertial reference unit (IRU) for acceleration sensing, the new unit is called inertial measurement unit (IMU) [3].

1.2.2 Angle/Vector Sensors

Angle (or vector) sensors use multiple angles (or vectors), which are directly measured in the body-fixed frame, as reference vectors to determine the space vehicle's orientation [2]. The following five sub-sections present the most common sensors of that kind.

1.2.2.1   Magnetometers

A magnetometer is an electromagnetic sensor that measures the ambient Earth's magnetic field direction and strength within the sensor's fixed coordinates (body-fixed coordinates). A complete measurement consists of three mutually orthogonal sub-measurements of the magnetic field to create a three-dimensional vector space. The three components then have to be compared with the known reference components of the exact position of the satellite in orbit [7] (page 368). These reference components are defined for each point in orbit around earth and are accessible using standard magnetic field models like the International Geomagnetic Reference Field (IGRF) [2]. The most commonly used magnetic field models are based on the tilted-centered dipole model, which is depicted in figure 1-6.
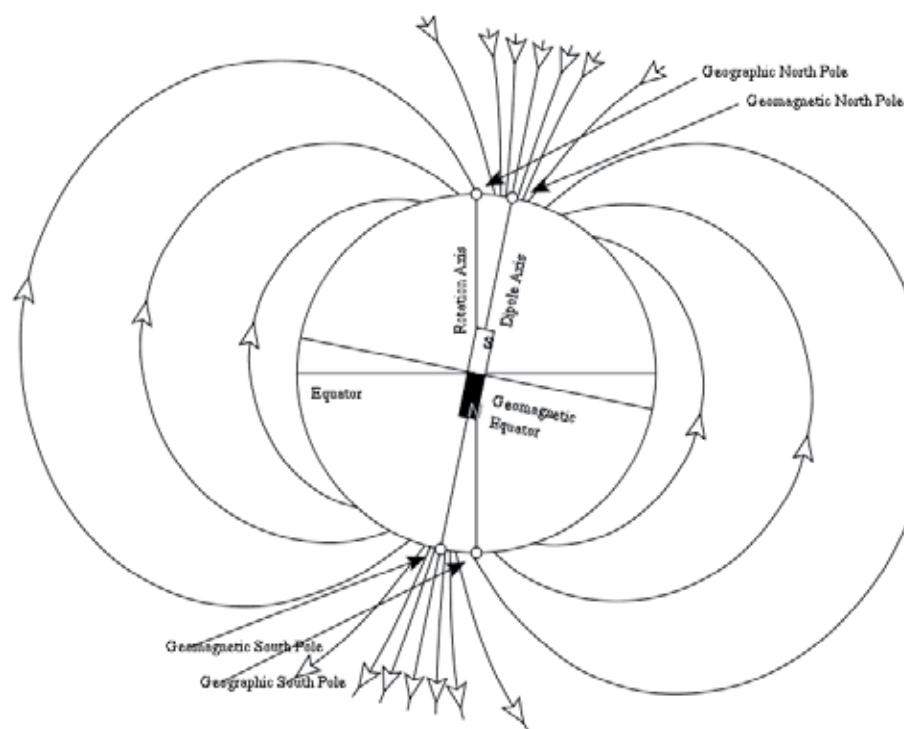
Figure 1–6: The tilted-centered dipole model of the Earth's magnetic field [10]

The spacecraft's attitude can be derived from the difference between the measured components in the body-fixed coordinates and the components taken from the magnetic field model [7] (page 369). To be able to do this it is, as stated before, necessary to know the exact position of the spacecraft. The two major drawbacks of a magnetometer are therefore that the exact position of the satellite has to be known to calculate attitude information and that even then only two out of the three rotation

angles can be measured at any one time (no angle information around the magnetic field lines). Only after a full orbit can a three angle attitude be estimated as the local magnetic field vector changes with respect to the LGCV frame over time. This does not work for an equatorial orbit because the difference in frame orientation (over time) changes as a function of latitude [2]. Figure 1-7 shows two different commercial models of a magnetometer.

Figure 1−7: Two commercial models of a magnetometer [2]

1.2.2.2 Sun Sensors

Sun sensors use the Sun as an external reference. They measure one or two angles between the body-fixed frame and the incident sunlight, while mostly using visible-light detectors [3]. They can be designed to fulfill different tasks including initial orientation acquisition, failure recovery of an attitude determination system or they could be part of (a subsystem of) the normal attitude determination system. Satellites with a solar array orientation system may use Sun sensors as a part of that system to allow for pointing of the solar arrays [3]. They can either be used on spinning spacecraft, like satellites with no or very limited attitude control, or on despun three-axis stable vehicles [7]. Although hardware designs vary widely, they are all designed to either provide digital or analog output signal formats [11]. Digital models mostly measure the incident angle of the sunlight coming through the slit entrance in a plane perpendicular to the slit [7] (page 365), which allows for the determination of one angle with a discrete output. To obtain a vector within the body-fixed frame pointing at the Sun, two Sun sensors are mounted orthogonally on each side of the space vehicle. Digital Sun sensors have a resolution measured in binary bits. The digital sensor in figure 1-8 below has a resolution of four bits as a result of the four separate detector elements.
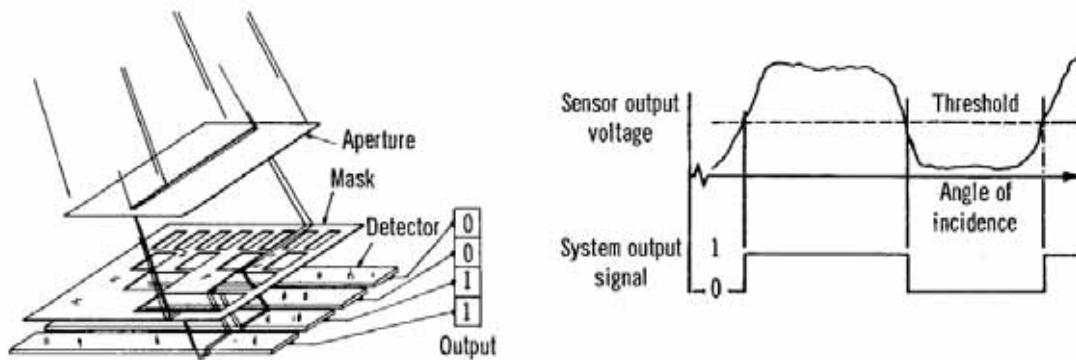
Figure 1–8: Digital Sun sensor with sensor output voltage and signal [11]

An analog Sun sensor outputs a continuous function of the angle of incidence [11]. Figure 1-9 depicts an analog sensor with two separate photosensitive elements. The difference in the current outputs of the two elements is measured and translated into the incident angle. If the difference is zero, the null point of the sensor is reached [11]. An aperture plate could also be used instead of the lens.
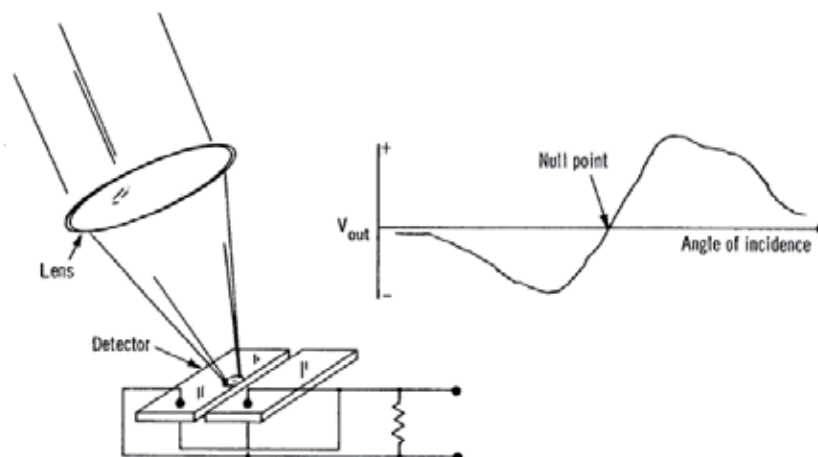
Figure 1–9: Analog Sun sensor with output voltage [11]

It lies in the nature of a Sun sensor that an unobstructed field of view (FOV) to the Sun is necessary. It can under certain circumstances be a challenge to provide for the clear view of the Sun sensor, especially when the spacecraft has a lot of external components. In addition to that most orbits around Earth (especially low-Earth orbits) include eclipse periods when the Sun is not in the FOV of the space vehicle. This loss of orientation data has to be compensated for by other sensors to maintain attitude determination [3] (page 371).

1.2.2.3   Horizon scanners

Horizon scanners have the ability to define the position of the horizon on each side of a spacecraft in an orbit around Earth, which enables a computer system to precisely define the nadir point. This method is especially reasonable for space vehicles in LEO (low-Earth orbit), where the cone angle of the Earth, which depicts the spacecraft's view of the Earth, will always be greater than 120° [7] (page 367). Most horizon scanner models are infrared devices that detect the contrast between the cold of deep space and the heat radiation of the Earth's upper atmosphere [3] (page 375). They make use of the atmosphere's CO_2 band, which radiates infrared light (15 µm wavelength) day and night and is, because of its thin layer, well defined in altitude. Its radiation is also not affected by clouds. These characteristics make the CO_2 band a reliable reference for attitude determination. Models range from rather simple narrow FOV fixed-head types (also known as pippers/horizon crossing indicators) to the more complicated scanning horizon sensors. Pippers are used on spinning spacecraft and measure Earth phases as a rising pulse and falling pulse as the pipper encounters going from cold space across the Earth and back into cold space [7]. Along with orbit and mounting geometry information several sensors are able to define the pitch and roll angle relative to the nadir [3]. Scanning horizon sensors use a rotating mirror or lens to augment the spinning of the spacecraft [3]. The difference between the expected pulse (relative to the orientation of the mirror) and the actual occurring pulse gives information about the pitch angle. By using another sensor mounted orthogonally, roll information will also be available (see figure 1-4). It is not possible to determine yaw information using horizon scanners, because the Earth always appears circular to the spacecraft for every given yaw angle [7]. Figure 1-10 shows the concept of a scanning horizon sensor [12].
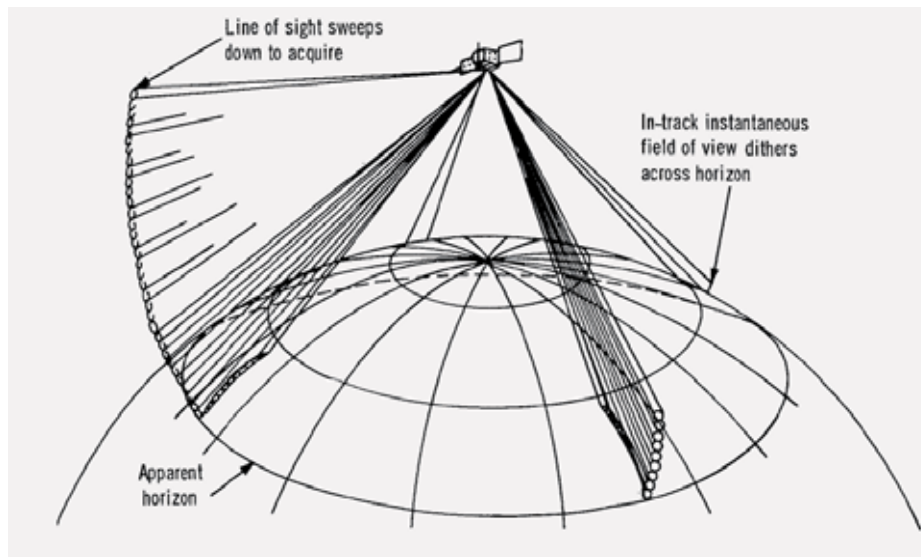
Figure 1–10: Concept of a scanning horizon sensor [12]

The main drawback of a horizon scanner is the variation in altitude of the CO_2 band. It can vary by as much as 20 km from point to point on the Earth's surface and is affected by different times of the day and year as well. For spacecraft orbiting in LEO this limits accuracy to around 0.05° (unless taking into account the Earth's oblateness) [7].

1.2.2.4 Star Sensors

Star sensors are generally used for missions with the need of very high-accuracy attitude determination. Two types of star sensors are available, which are both based on image processing: star scanners for spinning spacecraft and star trackers for three-axes stabilized spacecraft. Scanners are restricted in their FOV by multiple slits. The attitude of the space vehicle can be derived from several star crossings (as seen through the slits by the scanner) [3] (page 374). Trackers on the other hand track fixed stars to derive attitude information. Some systems even identify the viewed star pattern to obtain orientation information [3]. Unlike the other sensors of this section, star sensors do not experience major constraints in accuracy but rather in the system itself. Star sensors are generally sensitive to bright light and could already be blinded by the light coming from other planets, not to mention the sun. This has to be kept in mind when integrating these heavy and costly units. Another operational problem is caused by the time gaps between star identification (and orientation). They can be up to half an hour long, depending on the amount of star sensors used and the

spacecraft's orbit [7]. For this reason star sensors are often combined with gyroscopes (see section 1.2.1.1) to provide for the high-accuracy (but low frequency) external reference that the gyroscopes lack [3]. Figure 1-11 shows a model of a star tracker by Ball Aerospace and Technologies Corp. [13].

Figure 1–11: Star tracker by Ball Aerospace and Technologies Corp. [13]

1.2.2.5 Global Positioning System (GPS)

To determine orientation information for all three axes using GPS signals, it is necessary to have at least three antennas mounted at different points on the spacecraft. The relative position of the three antennas in the Earth-centered frame is determined by resolving small phase differences of the wavelengths transmitted by satellites in high Earth orbit. Although this concept is a relatively economic (in terms of cost, power, size and weight) it does require the spacecraft to have a reasonably large baseline, which often poses a limit of accuracy. Multipath effects due to reflections off vehicle components can add to the inaccuracy. Until now, they are mostly used in low-accuracy applications or as back-up sensors. [3,7]

All sensor data (section 1.2.1 to 1.2.2) that was taken from source [3] can be found on page 371-375.

1.2.3 Summary

For a direct comparison of the various sensor models, it is important to find the most vital parameters that have an impact on the mission requirements. Typically ADS subsystems have the most direct impact on the overall requirements in their size,

weight, power supply and accuracy. Another determining factor for the sensor selection is the application of the spacecraft. Table 1-1 briefly summarizes all sensor data of this chapter with respect to the given parameters, excluding size because of its great variability.

Table 1-1: ADCS sensors and their typical properties [2,3]

Sensor type	Typical accuracy (degrees)	Weight range (kg)	Power consumption (W)	Application
Horizon sensor	0.02 – 1.0	0.5 – 4.0	0.3 -10.0	Earth orbiters (spinner or three axis stabilized)
Magnetometer	0.5 – 3.0	<1.0	<1.0	Earth orbiters (three axis)
Sun sensor	0.005 – 3.0	< 0.5	0 – 3.0	Solar cell pointing, Sun vector determination
Star sensor	0.0002 – 0.08	2.0 – 5.0	5.0 – 20.0	High precision pointing
Inertial Measurement Unit	Gyro drift rate: 0.003 deg/hr – 1 deg/hr, acc.	1.0 – 15.0	10.0 – 200.0	High frequency inertial determination

1.3 Current Attitude Determination Systems for MOVE

As introduced in section 1.1, MOVE is a CubeSat in development at the Institute of Astronautics at the Technical University of Munich. Its current ADS consists of only a

Sun sensor subsystem, which uses four separate two-axes analog Sun sensors on each side of the cube to determine a reference (Sun) vector. It was developed and manufactured by the University of Denmark (DTU) and was later adapted for MOVE by Thomas Bickel (a TUM student) who designed a circuit board for the integration of the sensor at the Institute in Munich. Although the system does not include active attitude control of the satellite, it does use a passive configuration to correct disturbance torques and to align the satellite with the Earth's magnetic field. To achieve this, a permanent magnet and hysteresis rods are built into the satellite's structure [14]. While the permanent magnet aligns the satellite depending on the surrounding flux lines, the hysteresis rods dampen the effects of variations of the magnetic field by upholding (only over a certain time span) a magnetized state equal to the ambient magnetic field before the variation [15]. This procedure weakens the effect of the variation on the permanent magnet and therefore stabilizes the satellite in space.

The Sun sensor itself uses two pairs of rectangular photodiodes mounted perpendicular to each other. In figure 1-12 they are depicted as L (left) with R (right) and T (top) with B (bottom). The two diodes of one pair are separated by a small space between them. The abbreviation REF stands for the two reference diodes. The optical slit in the aperture plate is respectively parallel to the space between the diodes [16].
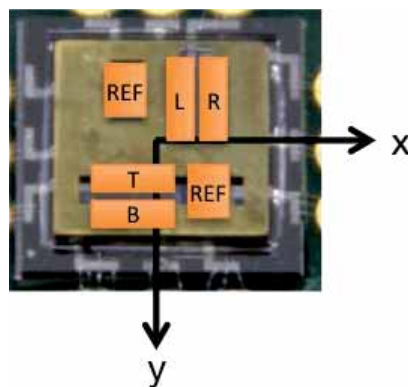
Figure 1–12: Pairs of diodes on the DTU sensor

Depending on the incident Sun angle, one of the two diodes of one pair will output a greater current than the other, which is partially covered by a shadow of the aperture plate. The two normalized quotients

$$I_{normalized,T,B} = \frac{T-B}{T+B} \text{ and } I_{normalized,L,R} = \frac{L-R}{L+R} \tag{1-1}$$

allow for independence of intensity and give direct information about the angles against the Sun vector in the body-fixed frame.

Its size measures only 14 x 22 mm. Figure 1-13 left shows the Sun sensor without its circuit board mounting compared to a pencil and the right image depicts the size constraints and the layout of the sensor mounted on its circuit board [16].
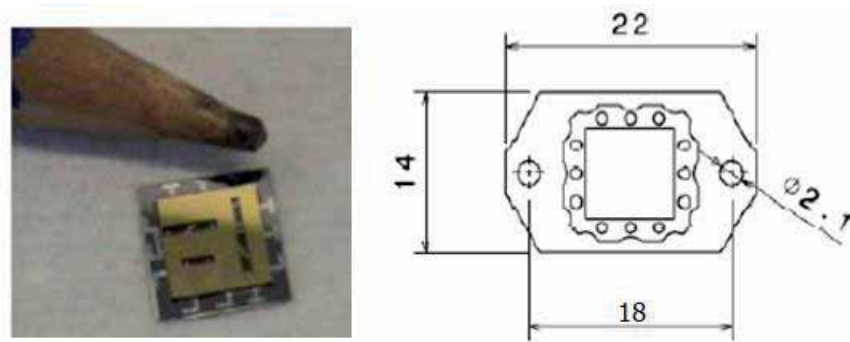
Figure 1–13: DTU Sun sensor size compared to pencil (left) and size constraints of the DTU Sun sensor [16]

The sensor's main advantages are its small size, low power consumption and its high accuracy, which is specified to ±1°. Nevertheless the sensor's layout is connected to a crucial disadvantage, which is related to the sensor's mounting. The set-up uses extremely fragile wire bonds (see figure 1-14) to connect the diodes with the circuit board. During the course of the MOVE project two of the four available sensors were already severely damaged and cannot be used any longer. The remaining two reliably working sensors will not cover complete attitude determination for the satellite and there are no more of these unique sensors available to acquire.
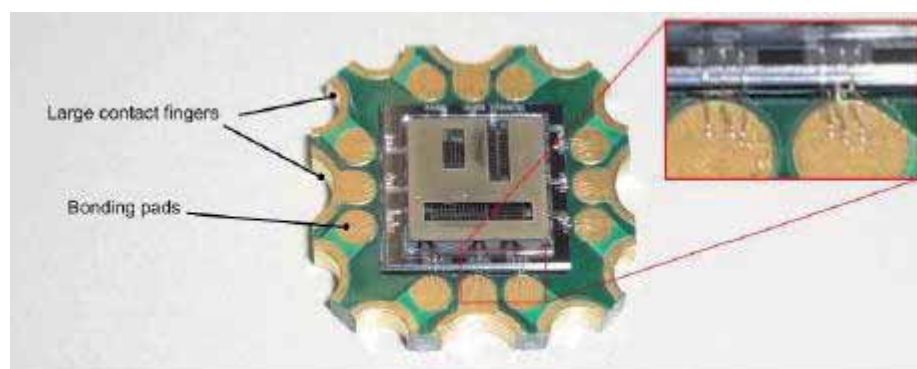
Figure 1–14: DTU Sun sensor connected to PCB via fragile wire bonds [16]

1.4 Statement of Work (Scope)

The circumstances described in section 1.3 were the initial reason for the development of a follow-up sensor for MOVE to replace the damaged system. They underline the urging necessity of a new attitude determination system for the project. The requirements imposed on a new system are to stay as close as possible to the structural set-up and properties of the DTU sensor and to deliver similar precision rates. An ADS is necessary for the MOVE satellite to enable analysis of its change in orientation over time and to evaluate newly developed solar cells, flown as experimental payload on the satellite. To be able to do this it is necessary to know the spacecraft's relative orientation to the Sun during experimentation. Another reason for the development of a follow-up sensor system is to support analyzing images taken from the onboard camera of the satellite.

2 Design and Construction of the PSD-based Sun Sensor Prototype

2.1 Requirements and Goals

The two specifications of an ADS that are most directly affected by the mission requirements are the spacecraft's required orientation and accuracy in determining that orientation. A satellite designed for Earth remote sensing would, for instance, require its ADS to deliver accurate Earth-pointing (nadir-pointing) for it to analyze the Earth's topography. Other determining factors that play an important role in the choice of a compatible ADS are the mission's specified fault tolerance, FOV requirements, available data rates and its redundancy [3] (page 375). Every mission has its own purpose and functionality, from which the requirements for its supportive sub-systems can be derived.

The purpose of the MOVE CubeSat is mainly to provide university students with hands-on experience in satellite engineering. Its secondary goal is to collect scientific data measured in space. On its way to space it will carry four newly developed high-efficiency solar cells, which were designed and constructed by AZUR SPACE Solar Power GmbH and provided to TUM by EADS Astrium. The 40 x 80 mm triple-junction solar cells have an efficiency of 30% and are of the type TJ Solar Cell 3G30C [17]. They will be tested as a part of the satellite's operations and later evaluated on the ground. The four cells are mounted on different sides of the cube and take up half the space of the side area each.

An accurate evaluation of the solar cells requires the satellite to have Sun vector coordinates available within its body-fixed frame, because they are vital for analyzing the cells' efficiency depending on the incident angle of the sunlight. In addition to that a suitable ADS should be able to perform initial attitude acquisition using an external reference. This is especially important because the satellite is ejected randomly from the carrier rocket. An external reference will provide reliable inertial pointing for the spinning body in space. As mentioned earlier, MOVE does not include an active attitude control system and therefore does not rely on high precision attitude determination, which is needed for the use of actuators. It is purely of scientific interest to obtain information about the satellite's spinning behavior in space.

Beside the accuracy and functionality requirements of the ADS, aspects of suitable integration are just as decisive. Since the goal is to replace an existing system, it will

be useful to adopt as many specifications as possible for a new sensor. This primarily implies staying within the size, weight, power and FOV constraints of the current system (section 1.3), while meeting all accuracy and functionality requirements imposed on the ADS by the mission itself.

The weight of the current system of 120 mg (excluding package and electronics) and its size of only 7 x 8 mm (14 x 22 mm including circuit board) are crucial constraints that have to be kept in mind when designing a new sensor system. For the third dimension of size, the MOVE structural configuration of the satellite allows up to 6 mm. Further, the current sensors use a FOV of 140° and only require power for communication components (all together: 9.48 mW) to deliver orientation information. Their allowed specified operating temperature ranges from -30 to +80 °C. To efficiently make use of existing communication software, it is reasonable to aim for the use of the same communication interface as it is used for the current system, which is based on Serial Peripheral Interface (SPI) communication. All these properties and the goal of achieving a similar specified accuracy (1° specified for the DTU sensor) are determining factors and requirements imposed on the design of a new sensor system [18]. The strict requirements of the sub-system are simultaneously closely related to the CubeSat specifications.

The final goal of the work described in this paper is to construct, characterize and test a new sensor system for the MOVE satellite and to later compare its properties with pre-developed systems. Figure 2-1 visually summarizes all mentioned determining factors for the design of a future sensor system for MOVE.
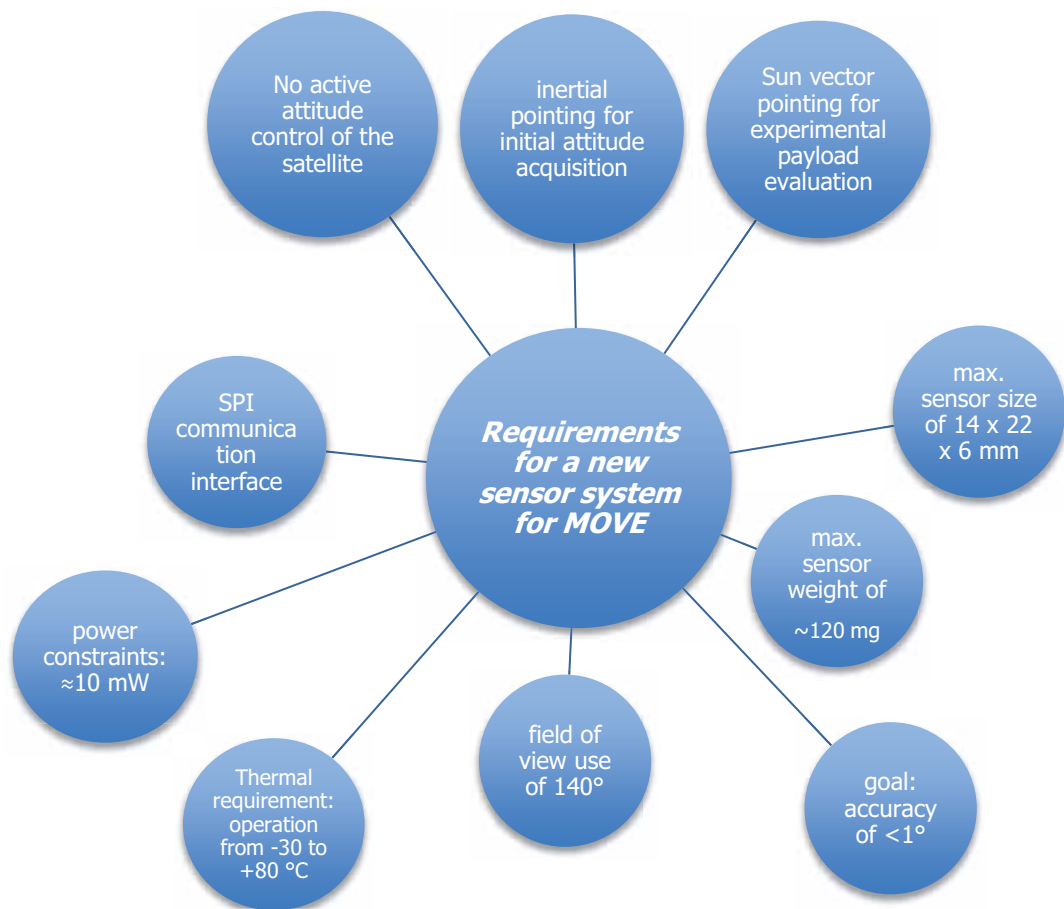
Figure 2–1: Determining factors of the requirements and constraints for a new sensor system for MOVE

2.2 Sensor Selection Process

To be able to determine the best, most cost-effective approach in sensor selection, a trade study was conducted. Referring back to section 2.1, it was defined as most important that the follow- up sensor is capable of providing inertial pointing for initial attitude acquisition and Sun vector pointing. (see figure 2-1) Table 2-1 correlates the different sensor types with their met MOVE requirements.

Table 2-1: Sensor types and their fulfilled (✓) MOVE requirements

MOVE requirements	Horizon sensor	Magnet ometer	Sun sensor	Star sensor	IMU
Inertial pointing	✓	✓	✓	✓	✓
Initial acquisition	✓		✓	✓	
Sun vector pointing			✓		
Max. size: 14x22x6 mm		✓	✓		
Max. weight: 120 mg			✓		
Accuracy goal: <1°		✓	✓	✓	✓
Thermal specifications	✓	✓	✓	✓	✓
Power: <10 mW		✓	✓		

Taken from table 2-1, the only sensor that fulfills initial acquisition and Sun vector pointing criteria is the Sun sensor. While the horizon- and star sensor can be used for initial acquisition (due to the use of an external reference), both the magnetometer and the IMU require external periodic recalibration to determine the attitude. The only reasonable solution for Sun vector pointing is the use of a Sun sensor, which directly determines the vector via external (Sun) reference. Therefore the sensor that best supports the main functionalities and goals of the mission is the Sun sensor.

The second step is then to examine whether the chosen sensor, which already fulfills all main criteria, complies with all other implementation requirements such as size, weight and thermal constraints. Table 2-1 shows checks for the Sun sensor for all secondary MOVE requirements. Nevertheless it has to be kept in mind that the Sun sensor has drawbacks in inertial pointing as well: it does not function during eclipse. While this heavily affects attitude determination, it does not have any effect on the

ability to evaluate the solar cells, because they also rely on sunlight to generate power. The most effective way to avoid loss of attitude determination during eclipse is to combine several sensors (e.g. Sun sensor and magnetometer), but since the goal of this project is to develop one follow-up sensor to replace the current model, this would be part of successive work. It was finally decided to develop a Sun sensor because it fulfills all mission criteria when the satellite is not in eclipse and there was no requirement to do so during the eclipse phases.

2.2.1 Available Sun Sensor Types

As stated in section 1.2.2.2, there are generally two different types of Sun sensors: analog and digital models. Various commercial aerospace companies offer Sun sensors to be acquired on the global market. These include the Adcole Corp., Ball Aerospace and Technologies Corp., EDO (Barnes) Corp., Ithaco Space Systems Inc., and Lockheed Martin [3]. Offers range from highly-sophisticated heavy-weight digital sensors to simple analog sensors, but none of the models are designed specifically for CubeSats and therefore do not meet the vital requirements regarding size, mass and power consumption. Other companies, like Clyde Space, provide entire modules for attitude determination and control especially for CubeSats, but do not offer single sensors that meet the MOVE requirements. One example of a single sensor offered by the ISIS CubeSat online shop is their "Miniaturised Analog Fine Sun Sensor," which meets all but the mass and size requirements. It weighs 50 g and its total size is 46 x 45 x 14 mm [19]. Hence, to best suit the needs of the MOVE mission, it was necessary to design a new sensor that is capable of using the current infrastructure designed for the DTU Sun sensor and fulfills all specified criteria.

Another approach, apart from developing a new system, is to test current components of the satellite itself on their ability to determine attitude. The only existing satellite component with attitude determination potential is a solar cell. Since any solar cell's output is dependent on the light's incidence angle, MOVE's experimental payload 3G30C features an opportunity to calculate this angle. This is based on the idea that the heat flux density, meaning the radiated energy per area and time on a solar cell, is directly dependent on the radiation's incidence angle [20]. The connection is expressed in the formula:

$$J = J_0 \cdot \sin(\theta), \tag{2-1}$$

where J is the actual radiant flux (radiant power) and J_0 is the radiant flux for an incidence angle (θ) of 90° (perpendicular to the cell's surface) [20]. The cell's ability to determine θ knowing J and J_0 with

$$\theta = \arcsin\left(\frac{J}{J_0}\right), \tag{2-2}$$

will, as explained later, be tested and evaluated along with a newly developed sensor system as it is introduced in the following.

2.2.2 Sensor Principle Solution for Development

In a coordinate system two points are needed to define a distinct vector. For the Sun sensor this means that a way to obtain the Sun vector is to determine two different points in body-fixed coordinates along the Sun's light beams (these can be considered parallel in Earth orbit due to the large distance between Earth and the Sun). To be able to do this with a changing incident angle of the light, one of the two determined points has to be variable depending on the angle. This can be achieved by using an aperture plate to extract only a fine beam with the hole defined as the fixed point, which the beam passes through. This principle is shown in figure 2-2.
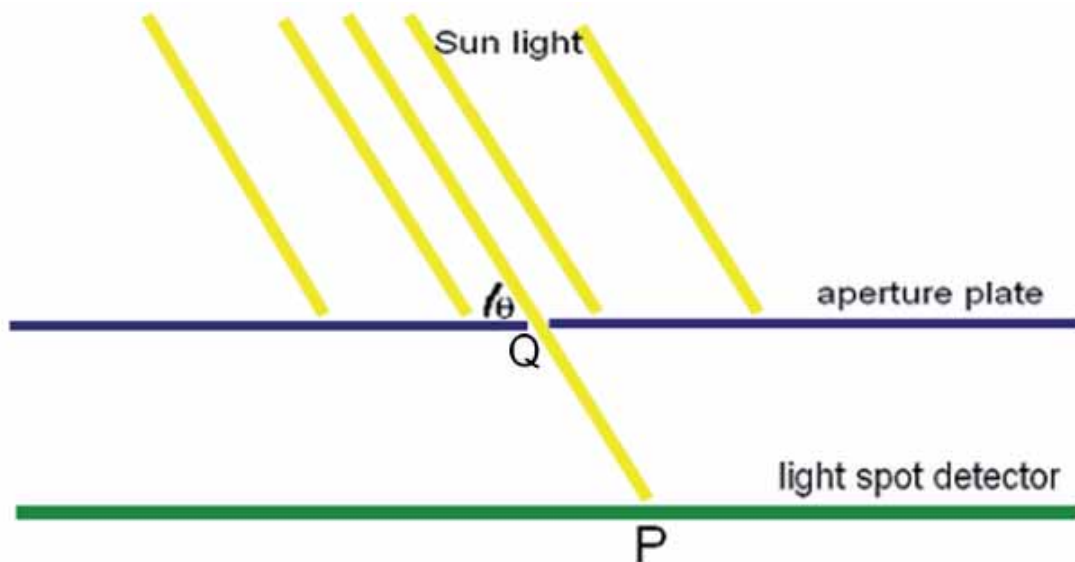
Figure 2–2: Sun sensor principle with aperture plate

The body-fixed coordinates of the point P and the hole (defined as point Q) in the aperture plate define the distinct Sun vector. In three dimensions the vector can be expressed as

$$\vec{s} = \begin{pmatrix} -x_P \\ -y_P \\ +z_P \end{pmatrix},$$ (2-3)

where the origin of the coordinate system is point Q (the hole), positive x goes to the right, positive y comes out of the paper plane, and positive z goes upwards. Point P changes with respect to the change in incident angle θ. Therefore one exact incidence angle is defined for every value of P.

To be able to determine point P in the coordinate system it was necessary to find a suitable instrument that can read out the exact position of the light spot in two dimensions. Section 2.3 introduces the Hamamatsu PSD, which was selected to fulfill this purpose.

2.3 The Hamamatsu Position Sensitive Detector

The Position Sensitive Detector (PSD) is an optical device offered for sale by the Japanese company Hamamatsu Photonics. Generally there are two kinds of different PSD types: one- and two dimensional detectors. The first kind merely determines the light spot position in one direction (e.g. x-axis) while the two dimensional device outputs information in two directions (x- and y-axis). To match the criteria stated in section 2.2, the two dimensional model was acquired, which will, combined with an aperture plate, allow for full three axis Sun vector determination. The PSD is normally used for the purpose of laser beam alignment or object tracking such as monitoring eye movement [21]. It was nevertheless chosen for this project, because it facilitates the required unique light spot determination traits. Figure 2-3 shows the two available PSD sizes (4 x 4 mm and 9 x 9 mm active areas).
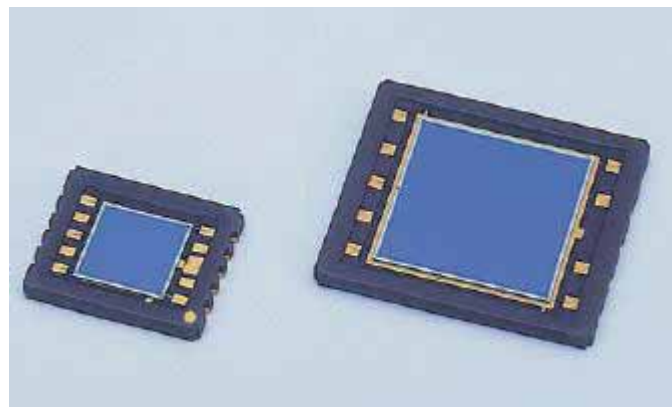
Figure 2–3: The Hamamatsu PSD (4 x 4 mm and 9 x 9 mm active areas) [21]

2.3.1 PSD Specifications

The two different PSD sizes shown in figure 2-3 are nearly identical in their specifications. To be able to work with and test the device, the larger version of the type S5991-01 was chosen. The reason for that is the fact that this paper primarily focuses on the proof of concept of the new system, where large components alleviate the process of troubleshooting and mechanical handling. For integration purposes (especially because of the smaller size and weight) all following set-up steps can be translated for application on the smaller version (type S5990-01), but are not carried out within this project. All following data and specifications on type S5991-01 were taken from the official data sheet provided by Hamamatsu [21].

Version S5990-01 measures only 8.8 (±0.15) x 10.6 (±0.2) x 1.26 (±0.15) mm (active area 4 x 4 mm) and is therefore well within the specified size constraints (see section 2.1). The PSD unit that is used for this project (sensor development) measures 14.5 (±0.2) x 16.5 (±0.2) x 1.26 (±0.15) mm and has an active area of 9 x 9 mm. The active area consists of a photosensitive surface to which four anodes are connected (see figure 2-4: X1, X2, Y1, Y2). The detector makes use of the photovoltaic effect. Depending on the position of the light spot on the active area, the four anodes measure different current values. With the recommended spot light size of 0.2 mm in diameter, the position detection error is typically in the range of only ±150 µm, while it has a position resolution of 1.5 µm. Figure 2-4 depicts the PSD's dimensional outlines (type S5991-01).
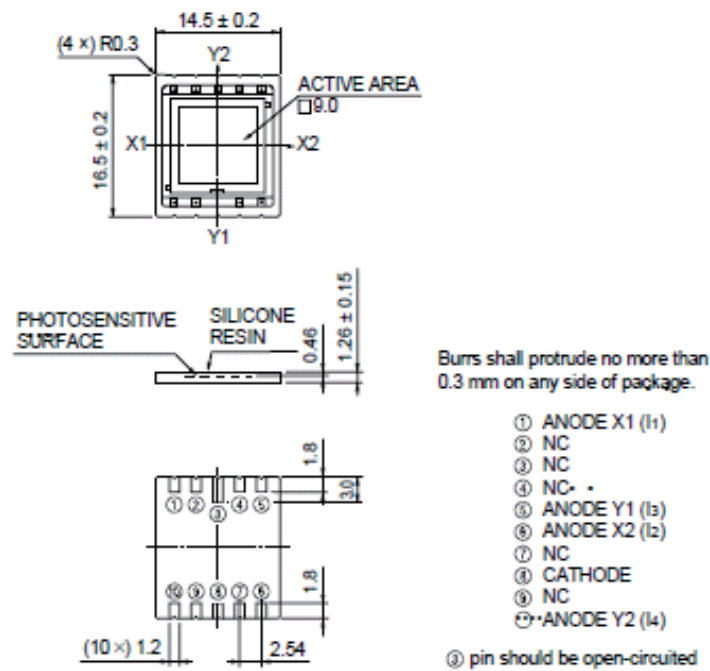
Figure 2–4: Dimensional outlines of the PSD (type S5991-01) [21]

The measured spot light position in x-direction is calculated using the given conversion formula:

$$\frac{(I_2+I_3)-(I_1+I_4)}{(I_1+I_2+I_3+I_4)} = \frac{2x}{L}. \tag{2-4}$$

Similarly, the position in y-direction is obtained using the following formula:

$$\frac{(I_2+I_4)-(I_1+I_3)}{I_1+I_2+I_3+I_4} = \frac{2y}{L}. \tag{2-5}$$

I_1 equals the current measured by anode X1, I_2 equals anode X2, I_3 equals anode Y1, and I_4 equals Y2 (see figure 2-4). L is a constant and has the value of 10 mm. The values of x and y are the spot light position coordinates P(x;y). Because the two equations are ratios, light spot position determination is independent of the intensity of the incidence light.

The PSD generally works with visible light, although its peak sensitivity is reached with light of the wavelength of 960 nanometers, which is outside the boundaries of human perception. Its spectral response range covers all light from 320 to 1100 nm wavelength. Figure 2-5 depicts this range in relation to the reached photosensitivity in $\frac{A}{W}$ for each wavelength. All electrical and optical characteristics are based on an operation temperature of 25°C and the recommended spot light size of 0.2 mm in diameter. The recommended operating temperature ranges from $-20°C$ to $+60\,°C$.
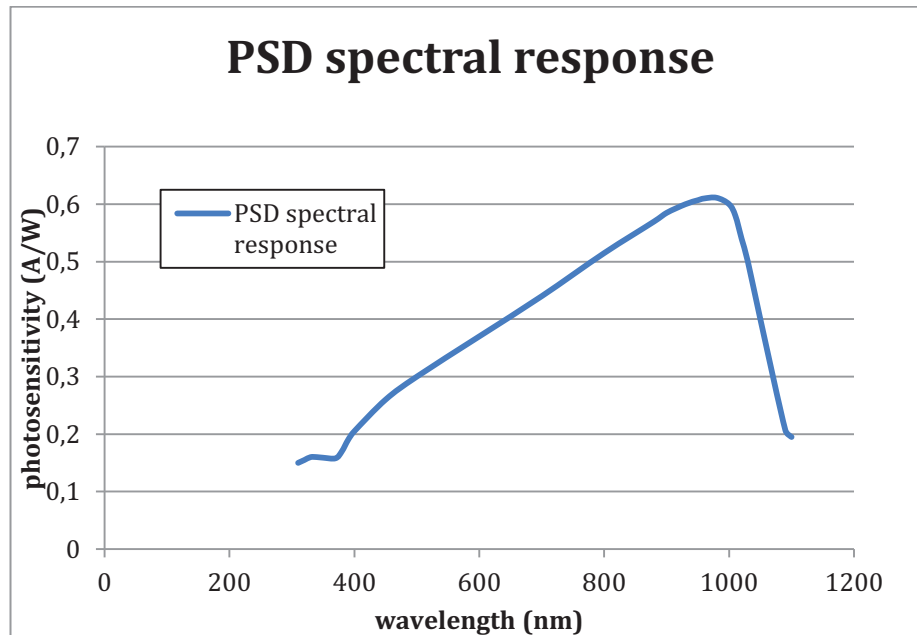
Figure 2–5: The PSD spectral response range [21]

The PSD can produce a saturation photocurrent of 500 μA (under the condition of a reference voltage of 5 V, using a 1 kΩ resistor and a 900 nm wavelength light beam), which is the maximum electric current light can evoke on the PSD.

To identify whether the PSD qualifies for application on the MOVE satellite, all its specifications have to be compared with the requirements imposed on the system. Table 2-2 matches the above mentioned data with the MOVE requirements of section 2.1.

Table 2-2: PSD characteristics at 25°C (spot light size ⌀0.2 mm) [21] and the MOVE requirements

Parameter	PSD S5991-01 (typical values)	MOVE Requirements	
Spectral response range	320 to 1100 nm	none	✓
Position resolution	1.5 µm (I=1 µA; f=1 kHz)	Sensor to be tested for 1° accuracy	
Saturation photocurrent	500 µA ($V_{ref} = 5\,V$; $\lambda = 900 nm$; $R_L = 1 k\Omega$)	none	✓
Operating temperature	-20 to +60 °C	To be tested in thermal-vacuum chamber	✓
Communication	SPI interface possible	SPI interface	✓
Power	Only for communication, same as the DTU sensor	9.48 mW for SPI communication	✓
Weight	To be measured with S5990-01	120 mg sensor	
Size	14.5 x 16.5 x 1.26 mm	14 x 22 x 6 mm *	✓

* This requirement is met by type S5990-01

The PSD has to be thoroughly tested whether it meets all of the in section 2.1 defined requirements of an ADS for MOVE, particularly with regard to its thermal specifications. Since there is no official thermal constraint for sensors on the MOVE satellite yet, the

current Sun sensor's thermal specifications (see figure 2-1) were taken as a reference. Because they are not fulfilled by the PSD, this aspect has to be analyzed in detail as part of the successive work. An option for expanding the operating temperature range if necessary is the use of the existing heaters for active thermal control.

The approximate 0.3 cm^3 PSD volume makes up around 0.03 per cent of the 1000 cm^3 the entire CubeSat measures. This does not include multiple sensors to cover all four sides of the satellite and the sensors' circuit boards. Whether the desired accuracy of the system, which is up to 1°, can be achieved with the precise position resolution of 1.5 µm over the 81 mm^2 active area will be tested in the course of this paper. All in all, the PSD qualifies in its main specifications for use on a CubeSat.

2.3.2 The Test Circuit Board for the PSD

To mechanically support and to electrically connect the PSD with other components used for communication it was necessary to design a suitable printed circuit board (PCB). PCBs use conductive pathways, which are etched from copper sheets laminated onto a nonconductive substrate [22], to supply power and to transfer data (in form of electric signals) from component to component. Since the PSD is predestined to use the same devices for communication as the DTU Sun sensor does (which are already installed on the CubeSat), these devices have to be installed on the test PCB as well. As this PCB is merely for testing, and not intended to function as a flight model, size constraints are not met for handling purposes. The following sub-sections give an overview of the three components needed for communication.

2.3.2.1 Operational Amplifier AD8554

Because the actual currents at the four anodes generated by the PSD are too small to be measured directly (max. 500 µA), a transimpedance amplifier is used to convert the current to a voltage, which is then amplified. As an operational amplifier (op-amp) the component AD8554 is part of the transimpedance amplifier circuit. This basic circuit is shown in figure 2-6. The resistor R is 680 kΩ., which yields and output voltage of up to 2.5 V. The AD8554 is a high precision, rail-to-rail op-amp and consists of a main and a secondary amplifier. It operates from 2.7 to 5 V with a single supply and withstands temperatures from -40 to +125 °C, which is within the specified range (see section 2.1). [23]
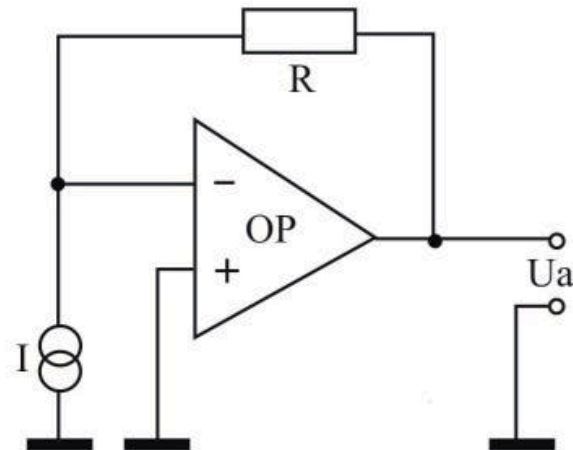
Figure 2–6: Transimpedance amplifier circuit [24]

2.3.2.2 Voltage Reference AD1582

The Analog Devices AD1582 is a low power, low dropout, precision band gap reference of 2.5 V. It is, just like the AD8554, specified to operate from -40 to +125 °C. The device has a low supply voltage headroom of voltages as low as 200 mV above the output voltage (2.5 V) [25]. It is needed to produce a reliably constant voltage irrespective of power supply variations or its loading. This voltage is used as a reference for measuring the voltage that is output by the transimpedance amplifier.

2.3.2.3 Microchip MCP3004

The Microchip MCP3004 is used on the PCB to convert the analog voltage comparison of AD8554 and AD1582 for all four channels into digital 10 bit values (A/D conversion). It has an SPI (Serial Peripheral Interface) bus to communicate with a central processing unit (CPU). The device operates with a voltage supply between 2.7 and 5.5 V and is specified to work within a temperature range of -40 to +85 °C [26]. It communicates with a CPU in a master-slave-relationship, where the MCP3004 is the slave component, and is connected to the CPU via four communication channels: Serial Clock (CLK), Serial Data Out (DOUT), Serial Data In (DIN), and Chip Select (CS). In addition it is connected to a +3.3 V power source and the ground (GND).

Figure 2-7 depicts all component connections on the PCB and its in- and output channels. All parts marked with a C are 100 nF capacitors, while the title R represents a 100 kΩ resistor. The connection diagram can be seen in the appendix section A2.
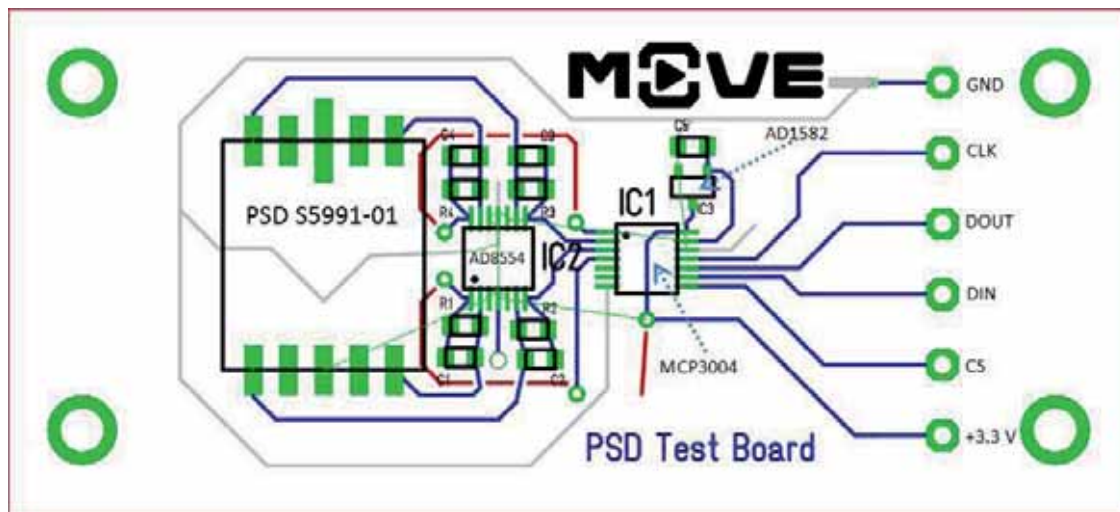
Figure 2–7: TARGET PSD PCB layout

The final PCB with the PSD integrated is shown in figure 2-8. It is the same PCB as seen in figure 2-7. All components apart from the PSD are mounted on the back side.
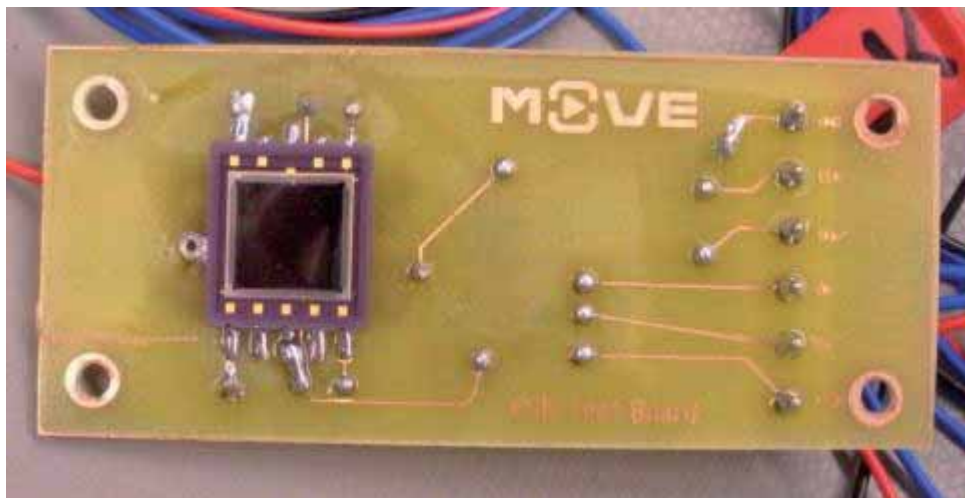
Figure 2–8: Final PCB for the PSD

2.3.3 The Aperture Plate

The sensor principle explained in section 2.2 works only with a fitting aperture plate that isolates a fine sunlight beam (see figure 2-2). The aperture plate designed for the PSD circuit board is a simple piece of bent sheet metal that is kept in place by spacers. To avoid light distractions on the PSD, the aperture plate has to be able to block the entire photosensitive surface from exposure to light other than light that passes through the hole. The hole itself is 0.2 (±0.05) mm in diameter and was drilled into a

thin (0.1 mm) plate to minimize light reflection off the edges of the hole. The size decision is based on the recommendation for spot light size in the Hamamatsu data sheet [21], which is also 0.2 mm. Because of the small distance between the aperture plate and the PSD in relation to the hole size, diffraction phenomena of the light beam can be neglected.
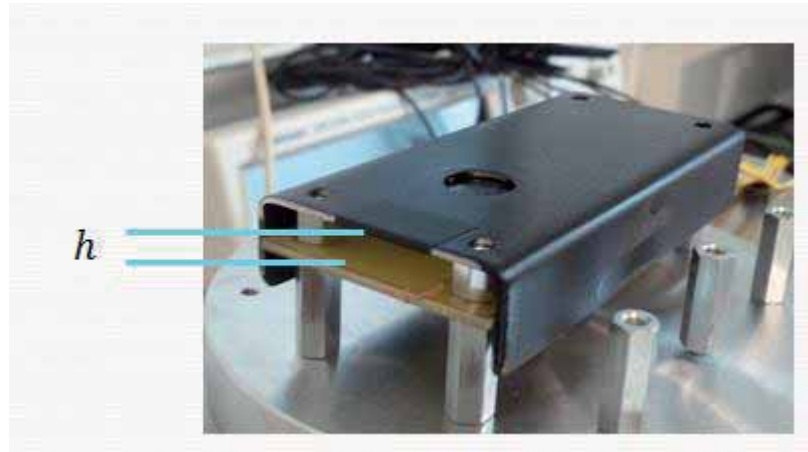
Figure 2–9: The aperture plate for the PSD

The distance between the PSD's active area and the hole (h) in the aperture plate defines the minimum incidence angle, for which the PSD detects light. The greater h becomes the smaller the field of view (FOV) of the sensor. The FOV (α) depending on h can be expressed using the following equation:

$$\frac{\alpha}{2} = \arctan\left(\frac{4.5}{h}\right). \tag{2-6}$$

Because PSD's active area has the form of a square with a side length of 9 mm, light spots in the corners will entail a greater FOV, while light spots at the edge half way across the sides yield the α FOV (in degrees) expressed by equation (2-6). Exemplary, for h = 5 mm the FOV angle is roughly 84°. To achieve a FOV of 140° (α=140) as it is specified in section 2.1, h has to be as small as 1.64 mm. With this assembly, the Sun vector can be obtained for any incidence angle within the specified FOV using formula (2-3), where z_P equals the magnitude of h.

3   Sensor Verification Method

3.1   Evaluation Process

All in all, three different sensor systems will be tested and compared in their performance. These include the current DTU Sun sensor (see section 1.3), the PSD-based Sun sensor (see section 2.3), and the experimental solar cell payload (see section 2.2.1). When testing, all three methods are evaluated under the same circumstances, so an accurate conclusion on which type qualifies and substitutes the DTU sensor best, can be drawn. The following sections introduce the methods and materials utilized for sensor validation.

3.2   Simulation of Satellite Orientation Positions in Space

As stated in section 1.3 the MOVE satellite does not have an active attitude control system. It merely relies on its passive system to align it along the Earth's magnetic field lines. In addition to that it is randomly ejected from its launch vehicle into orbit, which does not allow for initial information about rotational behavior. In this situation, the Sun sensor can be used to acquire attitude information. To be able to rely on the sensor's ability to perform this function in space, it has to be thoroughly tested on Earth before launch. The simplest way to do this is to simulate possible satellite orientations relative to the Sun (light source), which are then compared to the sensor's output data. This also allows for specification of the accuracy of the sensor.

For this purpose, a motor setup, which was developed by the Institute of Astronautics at the Technical University of Munich, was used. It was originally built for the Lightweight Intersatellite-Antenna (LISA) project. The LISA motor setup is capable of rotating a platform around two axes, which simulates two of the three possible satellite rotations around pitch, roll and yaw. For antennas, rotation equal to compass bearing change is called azimuth, while the elevation angle reflects the attitude of an observed object [27]. (Note: these definitions are used because the motor is usually utilized to point the LISA antenna) Figure 3-1 shows the LISA motor setup with its axes.

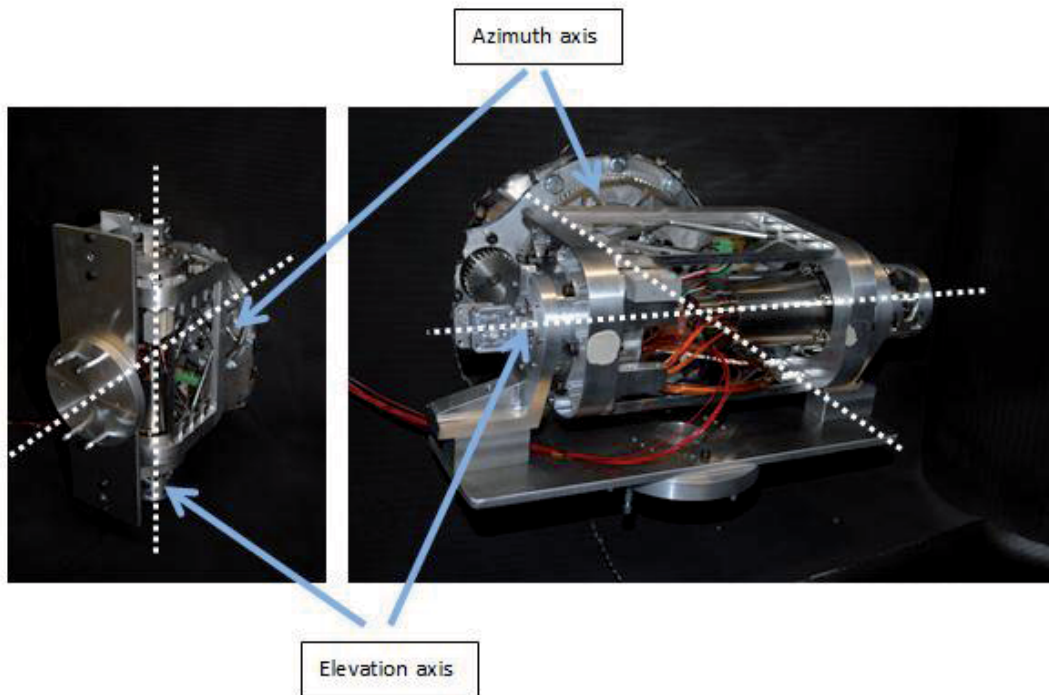*Figure 3–1: LISA motor setup with its two axes for rotation*

The rectangular platform (middle) with mounting bolts (left) and the circular interface (right) were specially designed with the CAD (computer-aided design) software CATIA (by Dassault Systèmes) to fit the mounting needs of the PSD sensor's PCB (see section 2.3.2). The parts are shown in figure 3-2.
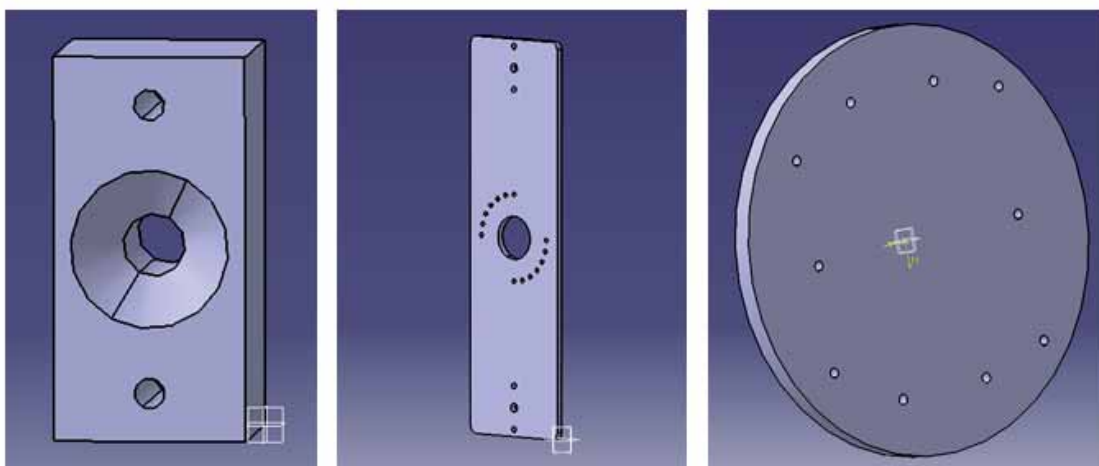

Figure 3–2: Sensor mounting parts (CATIA screenshots)

LabView Motor Control

As mentioned before, the LISA motor will simulate different satellite orientation positions for the sensors. To do this, it has to be programmed to run a certain sequence. The motor is controlled via Trinamic Motion and Interface Controller, which has an RS232 interface. This interface is included in a National Instruments PXI (PCI Extensions for Instrumentation), which is a PC-based platform for measurement and automation systems. It is used as an electrical bus for interconnection of peripheral components (PCI) such as the LISA motor and is controlled through an external PC. Systems are developed using the National Instruments LabVIEW software. This setup is shown in figure 3-6.

The motor sequence is divided into seven parts; one for every 15° of azimuth change. For each azimuth position, the motor rotates the platform with the sensor by 180° around the elevation axis (90° in both directions). This covers every position, from which the sensor can detect light from a fixed light source, which resembles the sun. The 15° steps are used to evaluate the sensors' performance for different azimuth angles (different alignment with respect to the light source).

Figure 3-4 shows how this is implemented as a computer program or virtual instrument (VI) in LabVIEW. The following description requires a basic understanding of the LabVIEW graphical programming language. It is beyond the scope of this paper to include an introduction to this language, the reader may refer to the National Instruments Homepage (http://www.ni.com) for further information. All following numbers in parentheses represent positions on figure 3-4.

There are two variables that represent the setpoints to which the motors are commanded. These are initialized with 0° for azimuth and -90° for elevation (1). The values are written to two global variables (2) to send their information via another VI to the motor, which starts turning into the demanded position. To leave time for the turning process before giving new commands, the while loop (3) only stops, when both the commanded azimuth, and elevation position is reached. This is done by comparing two global variables for both axes: "Stellwert" (setpoint) and "Position". "Stellwert" holds the value of the position command, while "Position" gives the current position of the motor. One of each variable is used for every axis (4). The stop signal for loop (3) is therefore only given, when the two variables are equal for both axes and the motor

has reached its position. After the first loop iteration of the outer while-loop (5) this position is 0° azimuth and 90° elevation. The sensor will have recorded data during this first part of the sequence. In order to start the second part, the azimuth motor has to turn the sensor by 15°, while the elevation motor goes back to -90°, so it can turn the sensor around 180° during the following loop iteration. As a result, the "Elevation Stellwert" is negated after every loop iteration of (5), while the "Azimuth Stellwert" is only increased by 15° every second loop iteration. This is controlled by a case structure, for which a Boolean constant is inverted every loop iteration. The entire process is stopped after 13 loop iterations (7), out of which the tested sensor acquired data during 7 loops (set by global variable (8)). The global variable "Fast?" regulates the motor speed, which is faster during non-recording loops simply to save time. During recording loops the motor has a very slow set turning speed to allow for more data to be acquired by the sensor. This is due to the limited measurement frequency of the sensors. Figure 3-3 shows a flow chart of the slow and fast (recording and non-recording) parts with the corresponding commanded motor positions.
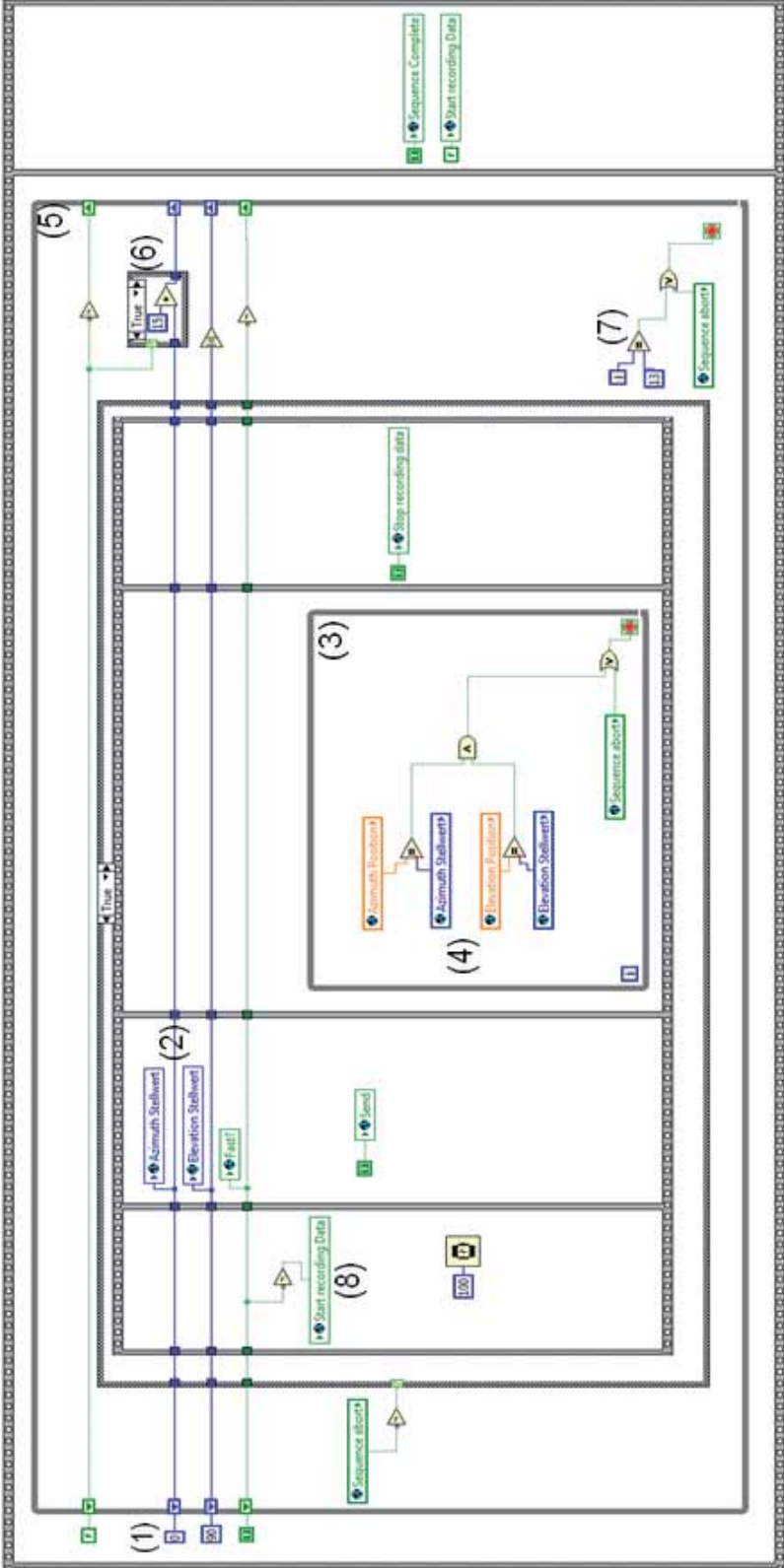
Figure 3–3: LISA motor position flow chart

Figure 3–4: LabVIEW motor sequence control VI

3.3 Sensor Data Acquisition and Logging

During the 7 recording loops of the LISA motor control explained in section 3.2, the tested sensors will actively acquire attitude data. While the PSD-based and the DTU Sun sensor both use the same infrastructure for communication via SPI with 4 data channels, the solar cell (see section 2.2.1) uses only one channel, which measures the voltage drop over a 2.5 Ω resistor. LabVIEW communicates with the 4-channel A/D converter via the PXI in a master-slave relationship using SPI. The obtained output data has to be logged for every sensor with respect to the actual motor position. This allows for a direct comparison between the actual and the measured orientation. Data logging is handled by the LabVIEW VI shown in figure 3-5. Again, all following numbers in parentheses reflect positions on the image.

As soon as the sequence is started, a new folder will be created and titled according to the tested sensor (1). Sensor data will only be written to the folder during recording-loops (see section 3.2), which is regulated by the Boolean variable "Start recording Data" (2). The variable is only set to "True" every second motor sequence loop (see section 3.2). Within the newly created folder the system creates a file named after the current azimuth degree (obtained by "Azimuth Stellwert") (3). After the entire sequence, there will be 7 files in the folder. After each value of the four channels and the actual azimuth and elevation positions are converted to engineering strings (4), they are concatenated (5) and written into a text file of the format ".txt" (6). Data is logged every 100 ms, which is regulated by a wait signal (7). The process is terminated when the sequence is either complete or aborted (8).
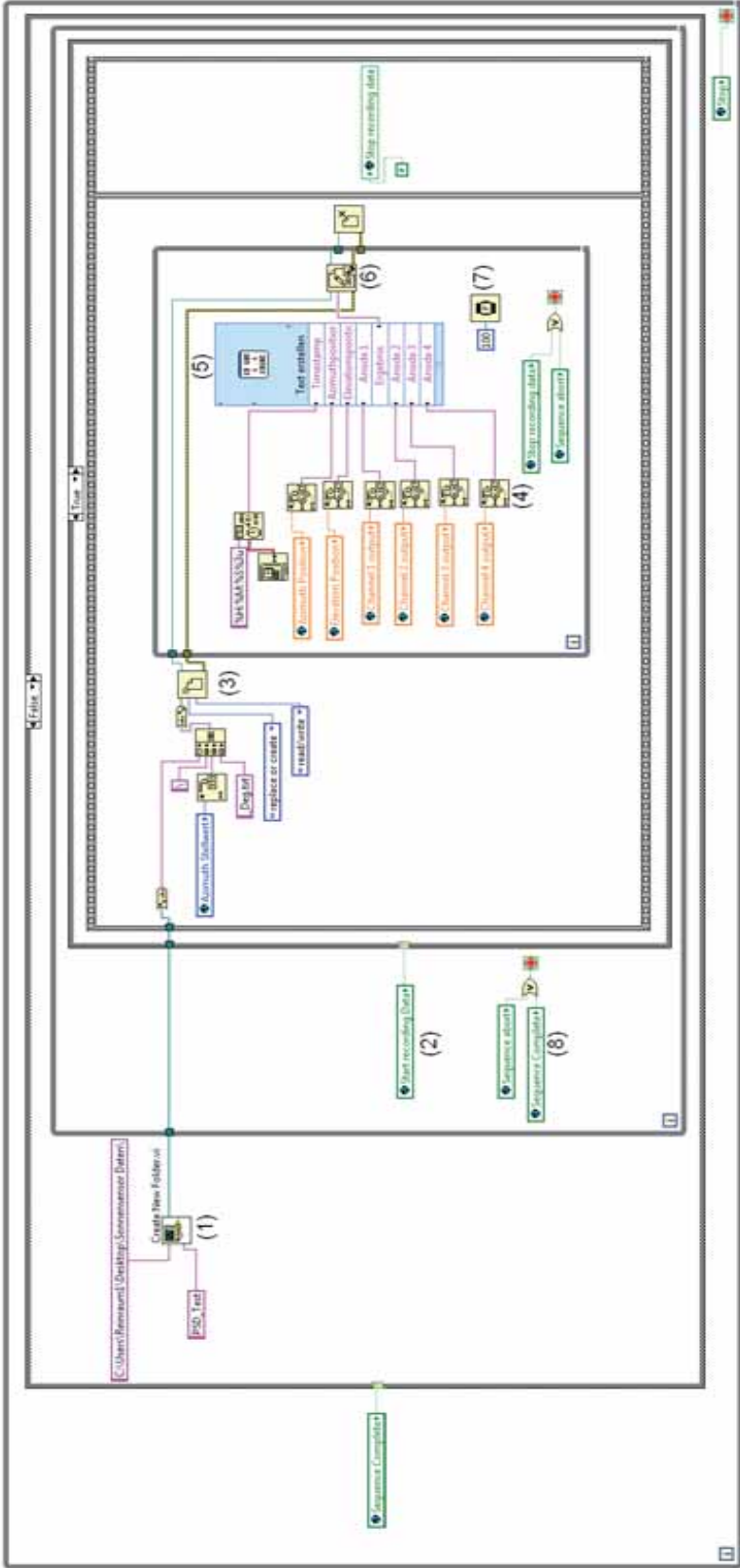
Figure 3–5: LabVIEW data logging VI

3.4 Experiment Control

The overall schematics of the data processing setup discussed above can be taken from figure 3-6. Data flow is always in both directions.

Figure 3–6: Schematics of the data processing setup

For observation and manual control of the testing process, an experiment control VI was created. The gauges show the value of the global variables "Azimuth Position" and "Elevation Position" (see section 3.2) at any time during a sequence. The front panel also includes the manually operated functions of sequence start and abort, as well as the command for the motor to return to its start position after a sequence has ended or was aborted. For each sequence the sensor, which is being tested, is selected from a drop down menu to give information on different procedures for data processing (see section 3.3). Figure 3-7 shows this front panel. The block diagram to this VI can be taken from the appendix section A3.
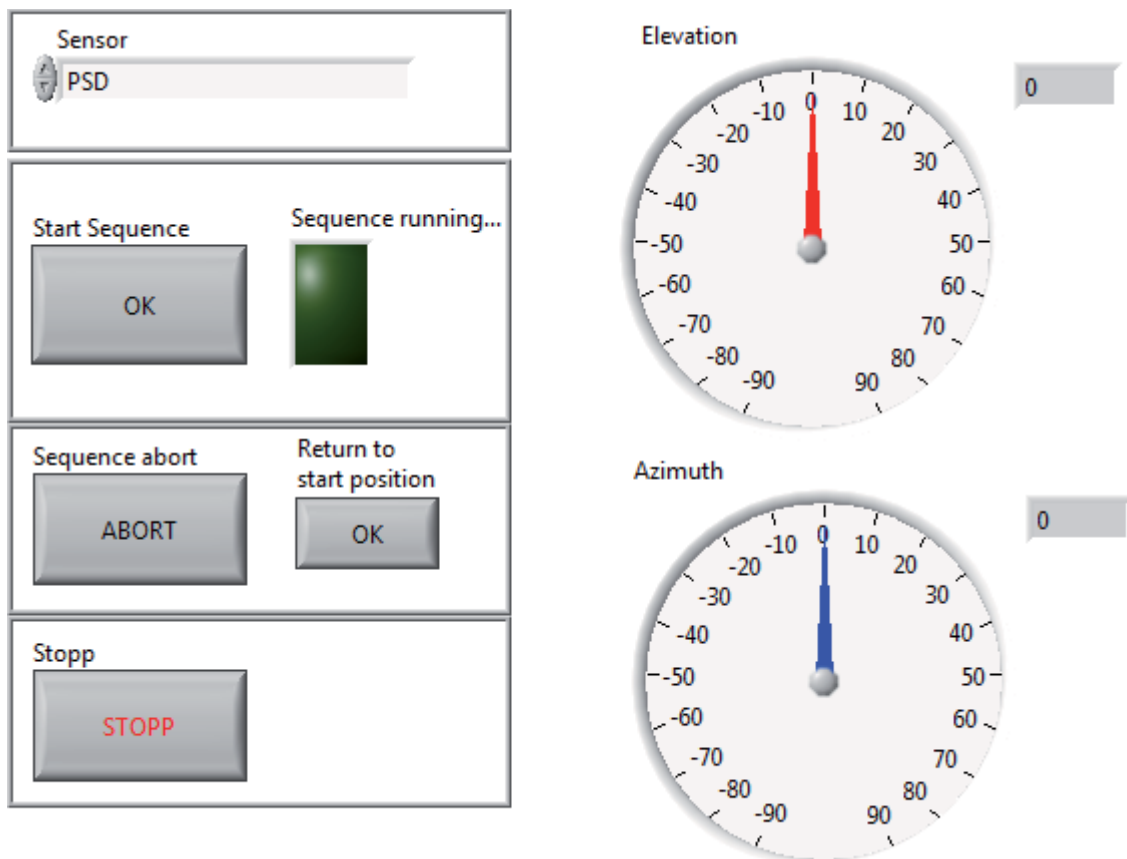
Figure 3–7: LabVIEW experiment control front panel

3.5 The Test Setup

3.5.1 Simulation of the Space Environment

For validation of the accuracy of a Sun sensor, it is necessary to test it in a similar environment as it will encounter in space. Obviously, there is no testing facility on Earth with the exact same environment as in space, but there are ways to simulate certain characteristics that have an impact on the functionality of the tested system. One of these characteristics is the darkness in space. In Earth orbit there is, idealized, only one light source: the Sun. To create this condition for the tested sensor, it has to be exposed to only one light source, which simulates the Sun. All other possible light sources (including reflections) have to be blocked.

This was realized using cartons as shields around the motor setup, leaving only one opening for a light source. To reduce light reflections off the cartons they were spray-painted matt black. This setup with the LISA motor is depicted in figure 3-8.
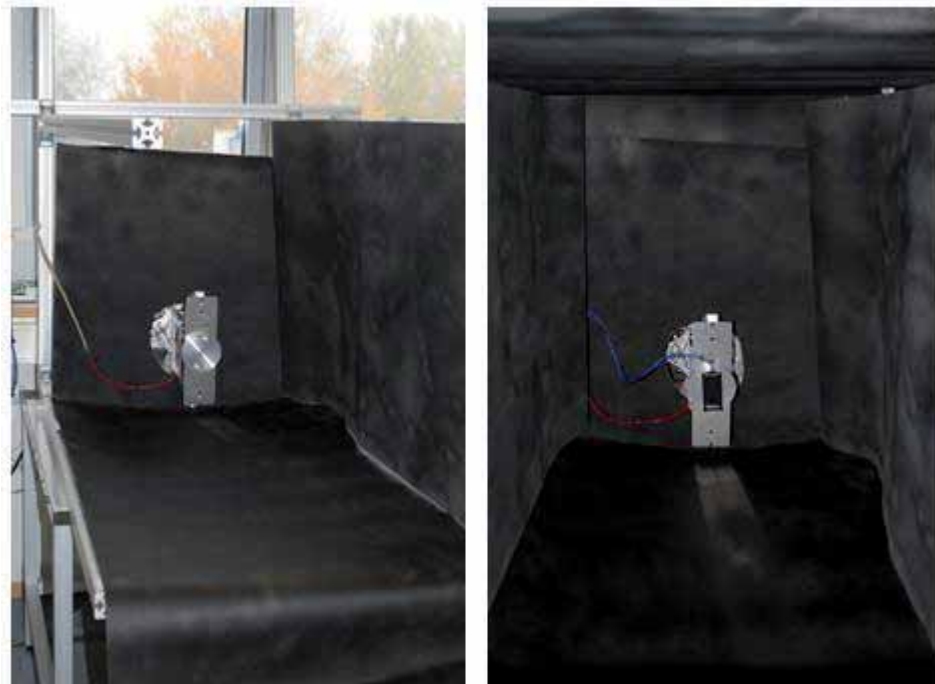
Figure 3–8: Light shielding setup for the sensor test

3.5.2 Simulation of the Sun

For the simulation of the Sun it was necessary to find a directed light source, with specifications similar to the Sun's. The total solar irradiance, which arrives at the mean Sun-Earth distance, is around $1.36 \frac{kW}{m^2}$ [28]. In Earth-orbit the Sun has a color temperature of around 6000 K [29]. Finding a light source that fulfills these criteria as well as possible was crucial for the test setup. Most real Sun simulators are very costly, which was the main reason for the choice of a conventional light. The following is a description of the selected light source for this project. It best fulfilled the criteria out of all considered and available lights.

The light source was rented at "TONEART mediavision" Augsburg, a supplier for camera equipment. It uses a 1.2 kW metal-halide lamp (HMI1200) and is called "Kobold DLf 1200S." It is supplied with a voltage of 220 V at 50 Hz, AC (internally converted to DC) and a current of 7 A. Its color temperature is specified to be about 6500 K, while its degree of efficiency is $92 \frac{lm}{W}$.

The lamp itself and the final setup with the lamp and the LISA motor is shown in figure 3-9, where it is placed 1.55 (±0.05) m away from the tested sensor mounted on the motor.
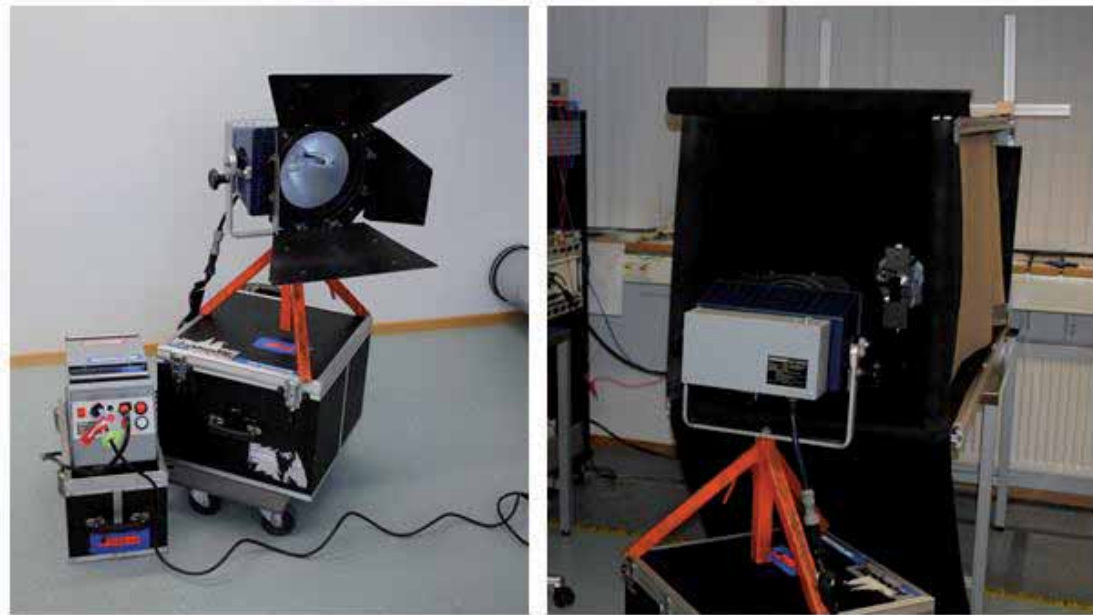
Figure 3–9: Kobold DLf 1200S metal-halide light for the sensor test setup

3.6 Sensor Data Evaluation

For sensor data evaluation, two different software programs were used: Microsoft Excel and MathWorks MATLAB. Both versions are developed similarly to serve the same purpose of plotting evaluation graphs.

3.6.1 Evaluation of the PSD-based Sun Sensor's Data

The PSD-based sensor outputs data in four channels. Since LabVIEW writes raw data with values of $Z \in [0;1023]$ into the text files, they have to be converted to attain the sensor's measured azimuth and elevation degree. The values of Z represent the comparison between the voltage output of transimpedance amplifier with AD8554 and the reference voltage AD1582 (2.5 V). Z is 1023 when the sensor is not illuminated, and 0 when the illumination evokes full-scale deflection. The values are distributed over the 2.5 V of reference in single steps, which entails an increase of Z when the voltage decreases:

$$2.5\,V \div 1023 = 0.0024437927663734\,V := q. \tag{3-1}$$

The constant q is therefore a single measured voltage step. This allows for calculation of the output voltage ($V_{amplifier}$) of the transimpedance amplifier for each channel:

$$V_{amplifier} = Z \cdot q. \tag{3-2}$$

Knowing $V_{amplifier}$, the actual current at each anode of the PSD, amplified over a resistor of 680 kΩ (R), can be calculated using Ohm's law:

$$I_{anode} = \frac{V_{ref} - V_{amplifier}}{R}, \tag{3-3}$$

where V_{ref} is the reference voltage (2.5 V). When I_{anode} is obtained for all four PSD anodes, the measured spot light position on the active area can be taken from formula (2-4) and (2-5).

The following steps explain the acquisition of the azimuth and elevation degree based on the sensor's measurements.

At first the light spot position on the PSD has to be calculated for the position of origin N (light beam perpendicular to the PSD's surface) using the above mentioned formulas. Next, the distance between point N and the calculated light spot position P (depending on the current motor orientation) is attained with:

$$\overline{PN} = \sqrt{(P_x - N_x)^2 + (P_y - N_y)^2} := d. \tag{3-4}$$

Finally, the arctangent of

$$\tan(\varepsilon) = \frac{d}{h} \tag{3-5}$$

gives the absolute value of the calculated elevation degree. Constant h is the distance between the PSD's active area and the aperture plate, which is depicted in figure 3-10. To differentiate angles in different directions and to obtain the real elevation angle from the absolute values, an if-condition was implemented, which analyses whether the measured x-position on the active area was smaller or larger than the value of the x-coordinate of point N. If the value was smaller, the calculated elevation angle is multiplied by -1 to yield a negative angle.
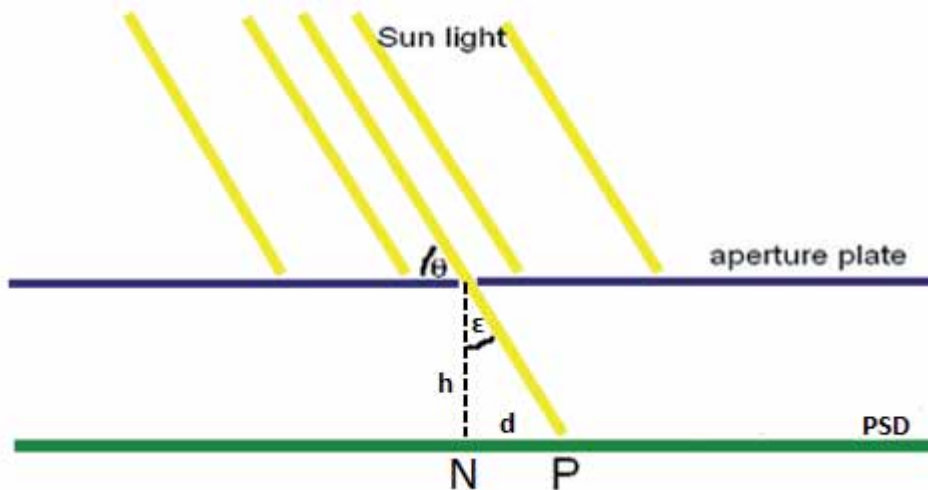
Figure 3–10: PSD-based Sun sensor principle with calculation variables

The azimuth degree is the same as the angle between $\overline{NP_1}$ (for $N \neq P_1$) in azimuth position 0°, and $\overline{NP_2}$ (for $N \neq P_2$) in the demanded azimuth degree. P_1 and P_2 are specific coordinates of P for the respective azimuth degree. In the following the variable a is the distance between P_1 and P_2 calculated analogical to formula (3-4). Using the law of cosine, the arccosine of

$$\cos(\alpha) = \frac{\overline{NP_1}^2 + \overline{NP_2}^2 - a^2}{2 \cdot \overline{NP_1} \cdot \overline{NP_2}} \qquad (3\text{-}6)$$

equals the azimuth degree based on sensor measurements. Figure 3-11 shows these points for exemplary values in the PSD's active area coordinate system. The implementation of these procedures in MATLAB (with comments) can be seen in the appendix section A4.

Figure 3–11: The azimuth degree on the PSD's active area (created using GeoGebra)

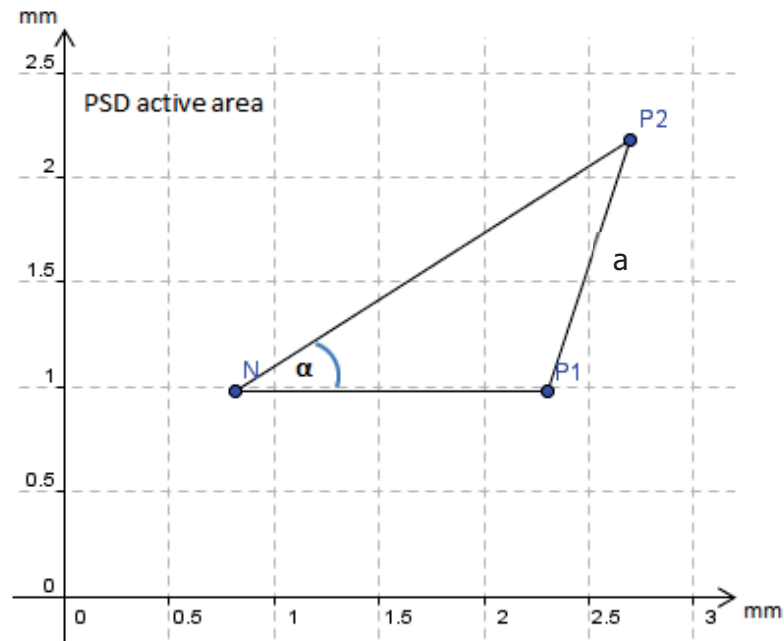### 3.6.2 Evaluation of the DTU Sun Sensor's Data

Just like the PSD-based sensor, the output data of the DTU sensor is divided into four channels using the same range of assigned values. Every channel equals the converted current evoked by one of the four diodes (see section 1.3). The conversion to voltage is carried out by a transimpedance amplifier (see section 2.3.2.1). As explained in section 1.3, the output values for Top and Bottom, and Left and Right respectively, are normalized using the two equations (1-1). Because both normalized values are within a defined range of]-1;1[, they have to be multiplied by 90. The reason for this is that the value of 0 is defined as full sensor illumination, which is reached when the motor is in elevation position 0°, while values of almost 1 signal no sensor illumination. The multiplied values are then plotted together with the actual motor orientation position, which are also obtained via LabVIEW (see section 3.2). This is done using Excel.

3.6.3 Evaluation of Solar Cell 3G30C Data

Unlike the two sensors above, the payload solar cell outputs data only in one channel, which has values of [0;32767] corresponding to voltages of 0 V and 10 V, respectively. The values are proportional to the voltage drop over a 2.5 Ω resistor. The voltage drop

is proportional to the current produced by the solar cell (max. 600 mA), which in turn is dependent on the light's incidence angle (see section 2.2.1). Formula (2-2), which allows for calculation of the incidence angle θ knowing the radiant flux, is converted to the following formula that expresses the angle's connection to the cell's output current:

$$\cos(\theta) = \frac{I}{I_0}, \qquad\qquad (3\text{-}7)$$

of which I is the measured current at θ, and I_0 is the current measured when the light is in the cell's zenith position. The currents are obtained via Ohm's law with a resistor value of 2.5 Ω. The arccosine of (3-9) yields the measured incidence angle. Since the calculated angles have different dimensions than the actual motor position, they are multiplied by 47.4 to fit the graph. This process is implemented in MS Excel.

3.6.4 Calculation of Sensor Measurement Error

To compare the sensors' performance in elevation angle determination with each other, the average measurement error (E) of the sensors' calculated data and the actual motor angle is computed. It is defined as the average distance (absolute values) of all data points from the real elevation angle within a certain FOV or range [30]:

$$E = \frac{\sum_{i=1}^{n} \sqrt{(\varepsilon_m(i) - \varepsilon_a(i))^2}}{n}. \qquad\qquad (3\text{-}8)$$

The formula, where n is the total quantity of sensor position measurements, ε_m is the measured (calculated) elevation angle, and ε_a is the actual motor elevation angle, directly reflects every tested sensor's accuracy in elevation angle determination.

4   Test Results

4.1   Test Phase One

The test setup for the first sensor test can be seen in section 3.5. In the following, the test results of each sensor are briefly summarized.

4.1.1   PSD-based Sun Sensor Test Results

For the first test of the PSD-based Sun sensor, spacers of 5 mm were used, which leaves a distance of 3.74 mm between the aperture plate and the active area (see section 2.3.3). The plot of the sensor's raw output data for azimuth 0° (shown in figure 4-1) shows two large bulges (1), which signal heavy illumination, with minima at motor elevation degrees around -30° and +30°. These unexpected bulges led to an incorrect calculation of the elevation degree (see figure 4-2). Figure 4-2 is a plot of the values of the actual motor elevation position and the elevation position calculated by the PSD, which would be identical if the sensor delivered perfect data. The calculation process is explained in section 3.6.1. The plot of figures 4-1 and 4-2 are very similar for all motor azimuth degrees (sequence parts). The test eventually did not deliver valuable results.
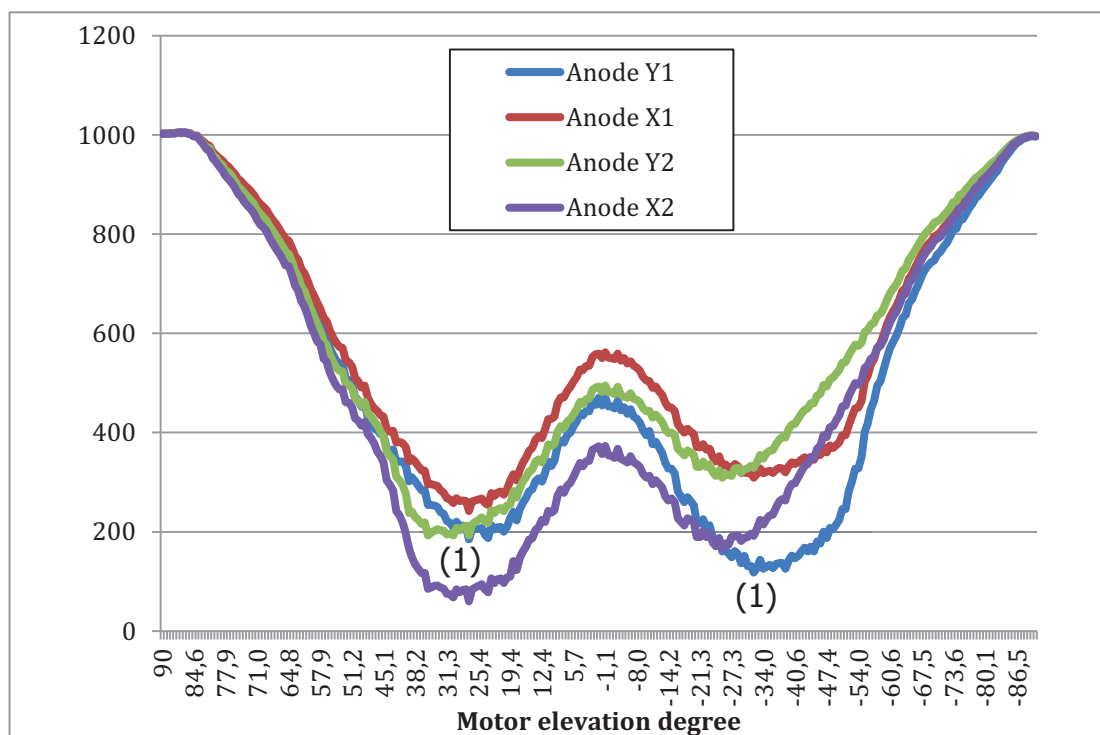

Figure 4–1: Plot of PSD Sun sensor raw data for motor sequence part 1 (azimuth 0°)
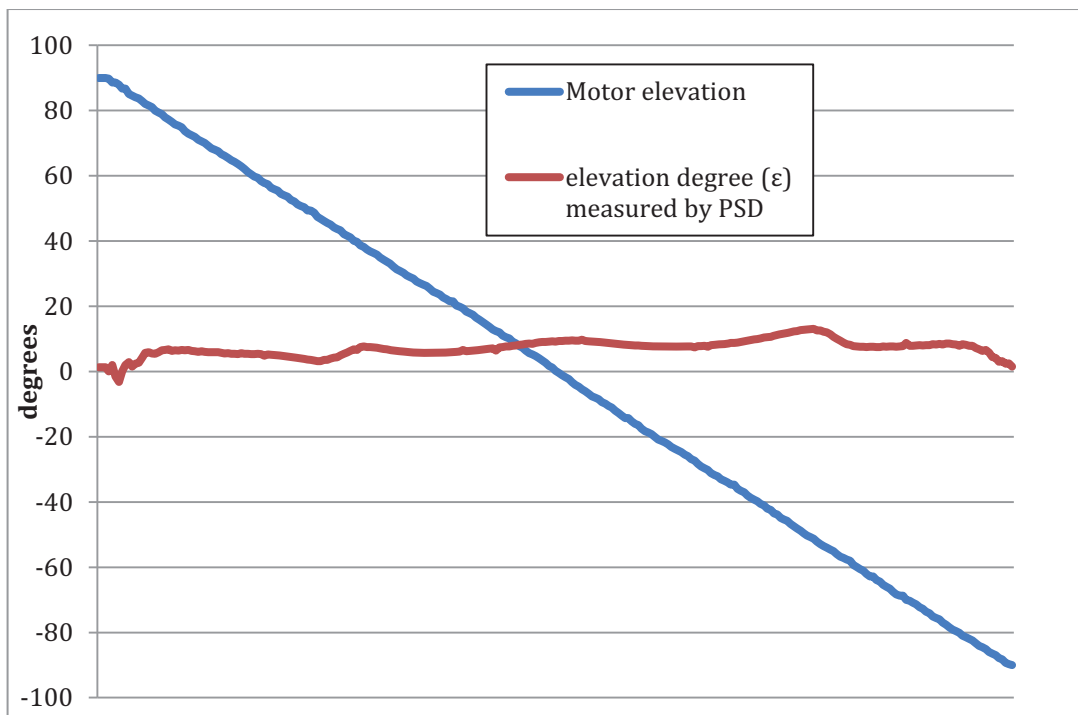
Figure 4–2: Elevation degree based on PSD measurements for motor sequence part 1 (azimuth 0°)

4.1.2 DTU Sun Sensor Test Results

Figure 4-3 shows the DTU sensor's raw data output of the four diodes (see section 3.6.2), again for motor azimuth sequence part of 0°. The normalized values multiplied by 90 of diodes T and B, and L and R respectively (see section 1.3), are plotted in figure 4-4. The fraction $\frac{90L}{R}$ represents the measured elevation degree (for motor azimuth 0°), while the fraction $\frac{90T}{B}$ represents the steady azimuth angle (roughly 6° due to the sensor's mounting tilt) (see figure 1-12). Within the sensor's specified FOV of 140°, it has a measurement error of 8.5° from the actual elevation motor position. As seen in the graph, the smaller the FOV is specified the smaller the measurement error becomes. For the motor elevation range of 50° to -40° (see section 4.2) the measurement error is 6.9°.

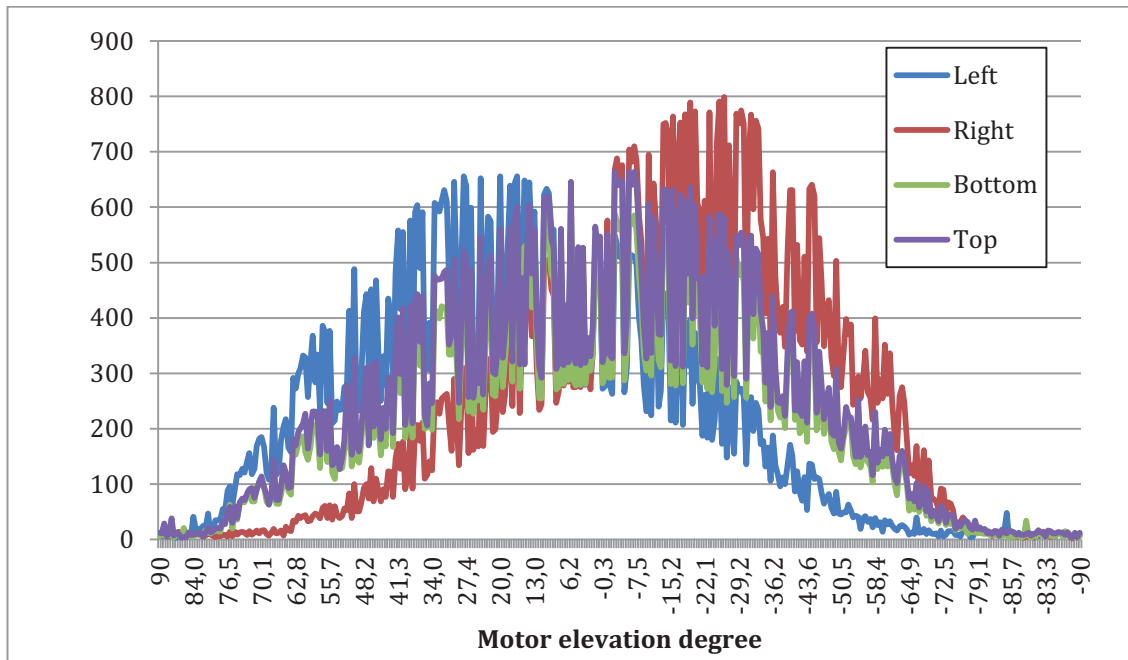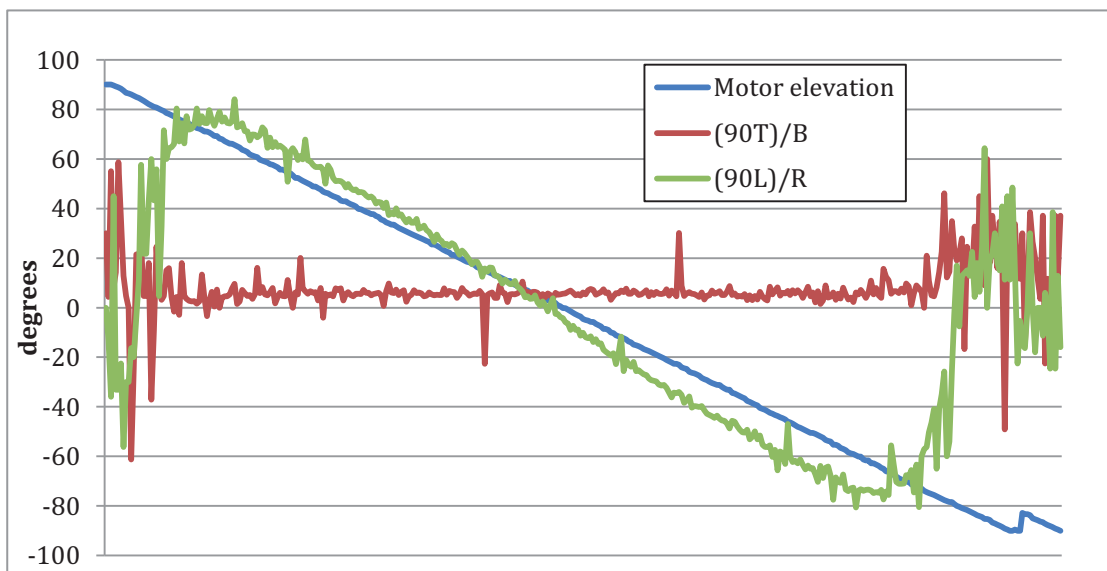*Figure 4–3: Plot of DTU Sun sensor raw data for motor sequence part 1 (azimuth 0°)*

Figure 4–4: Elevation degree based on DTU Sun sensor measurements for motor sequence part 1 (azimuth 0°)

4.1.3 Solar Cell 3G30C Test Results

Just like in the other two tests, the solar cell delivered almost the same data for every azimuth angle. Figure 4-5 shows the plot of the one-channel raw data for azimuth

position 0°. Because of high noise level of the output data due to measurements inaccuracies, a polynomial (power of 6) trendline (g(x)) was added to the graph.

g(x) = 6E-12x^6 - 9E-09x^5 + 6E-06x^4 - 0,0024x^3 + 0,3434x^2 - 6,4199x + 99,405
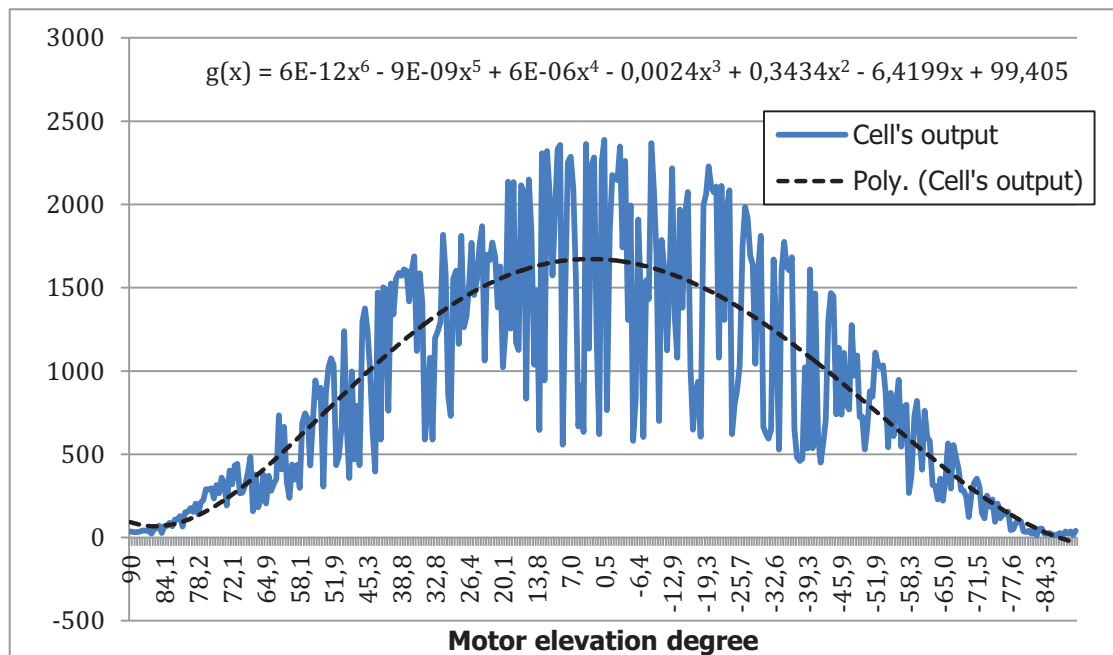
Figure 4–5: Plot of solar cell 3G30C raw data for motor sequence part 1 (azimuth 0°)

As a result of the noisy output, the calculated incidence angle of formula (3-7), which is depicted in figure 4-6, is based on the values of the trendline. The values are absolute because the cell cannot differentiate between a positive and a negative incidence angle (one angle output). For better comparison of the two graphs, the motor elevation is also plotted for absolute values only. Within a FOV of 140° the measurement error (with respect to the absolute motor elevation) is 2.1°. For the range between +50° and -40° (90° FOV) the measurement error is 2.3°.
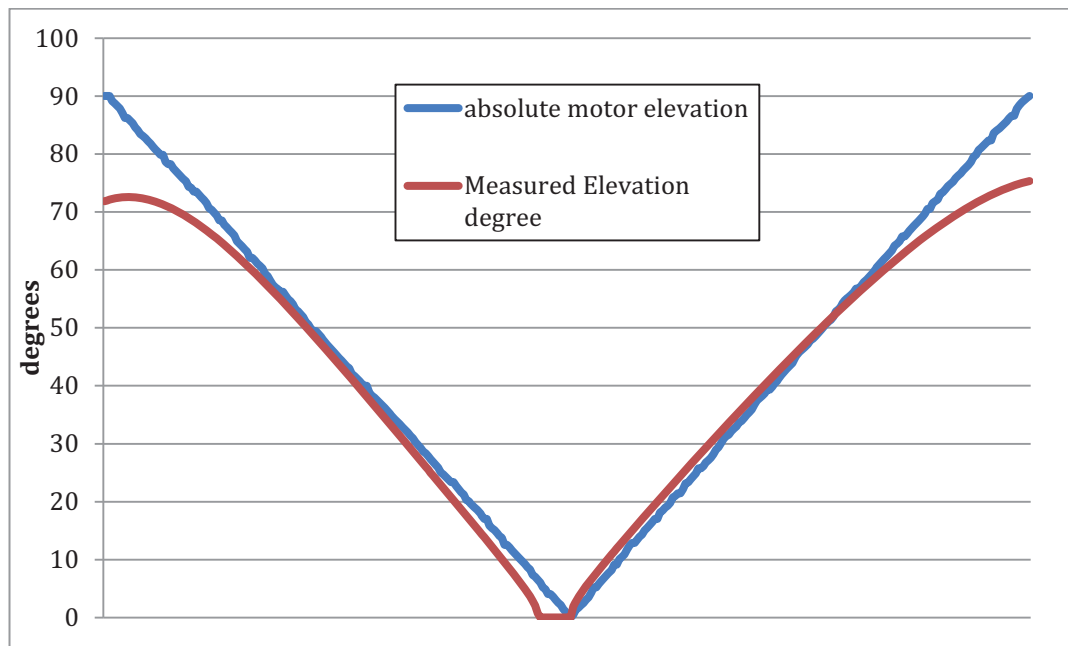
Figure 4–6: Elevation degree based on trendline of solar cell 3G30C measurements for motor sequence part 1 (azimuth 0°)

4.2 Test Phase Two

During testing phase two, the main focus was to enhance the PSD-based sensor's results. All other sensor results stayed the same as in test phase one. The sensor problems of the first test were found after a detailed analysis of all test setup components. The reason for the erroneous results was the sensor's light shield, which did not fulfill its purpose of protecting the sensor from unintentional exposure to light. It was the motor's sensor metal mounting platform that caused backlighting of the circuit board through light reflection. This entailed full sensor illumination at motor elevations of around -30° and +30° (see section 4.1.1). The circled area in figure 4-7 shows the reflecting surface. This problem was solved using duct tape, which was taped all around the sensor to prevent the disruptive reflections (see figure 4-7).
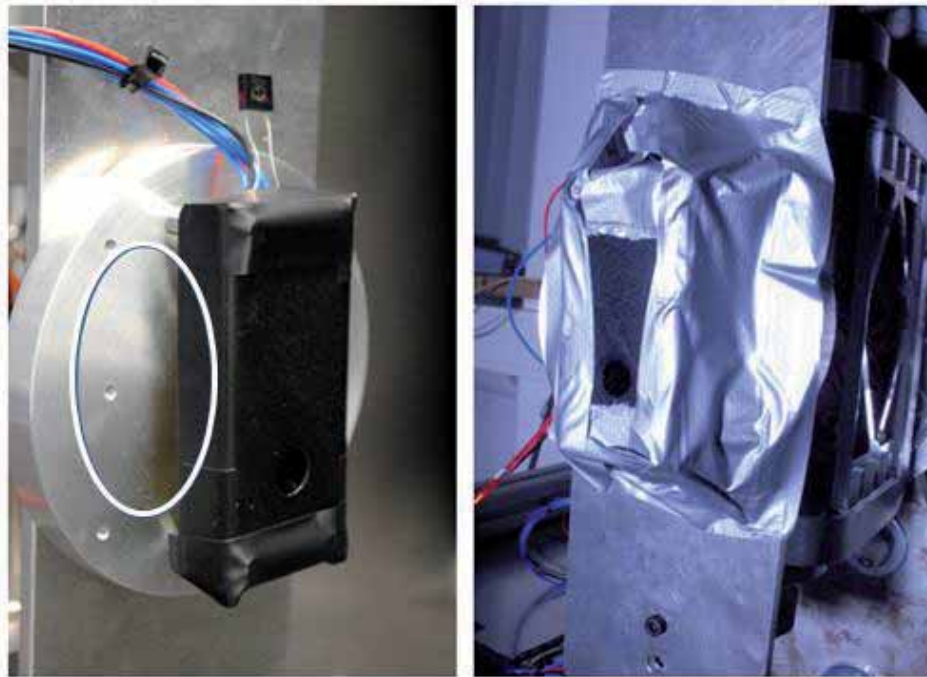
Figure 4–7: Solution of sensor backlighting problems due to reflection

This new setup (using the same spacers) yielded entirely new data. The raw data can be seen in figure 4-8, while the calculated elevation and azimuth degrees are shown in figure 4-9. Both graphs represent motor sequence part 1, as in section 4.1. The results are again similar for all azimuth positions. The measurement error between motor elevation position +50° and -40° and the calculated elevation position in that range is 1.08°. In the same confinement the calculated azimuth angle has values of roughly 0.6° (excluding the midrange 180° maximum) that reflect the measured mounting tilt.

Figure 4–8: Plot of PSD-based Sun sensor raw data for motor sequence part 1 (azimuth 0°)

Figure 4–9: Elevation degree based on PSD Sun sensor measurements for motor sequence part 1 (azimuth 0°)

5 Performance Evaluation and Discussion

5.1 Motor Sequence Error

The reason for the identical results of sensor azimuth degree calculation for all motor azimuth positions is a minor flaw in the experim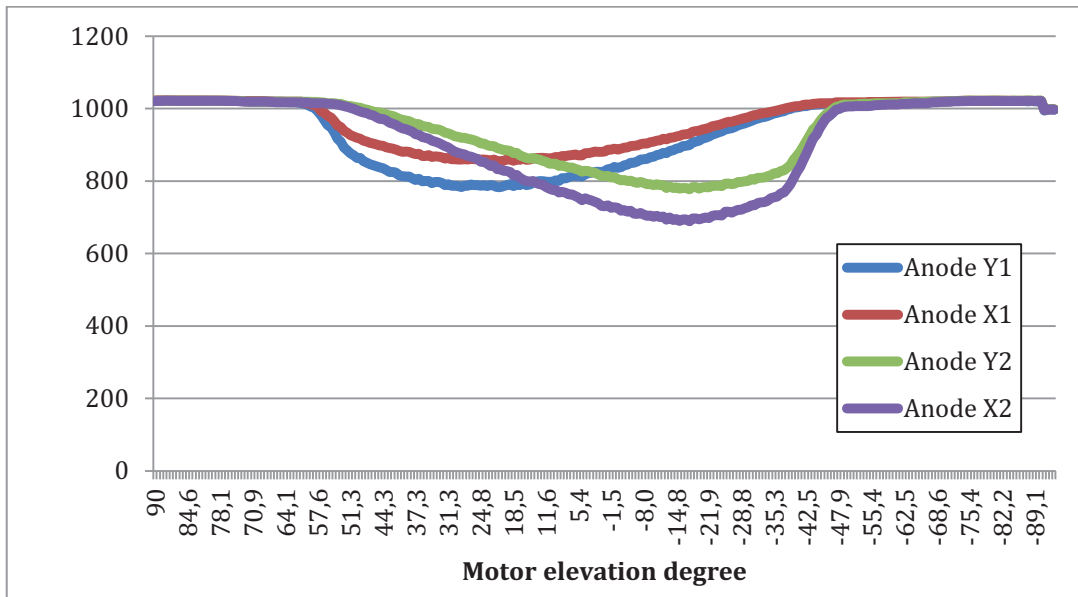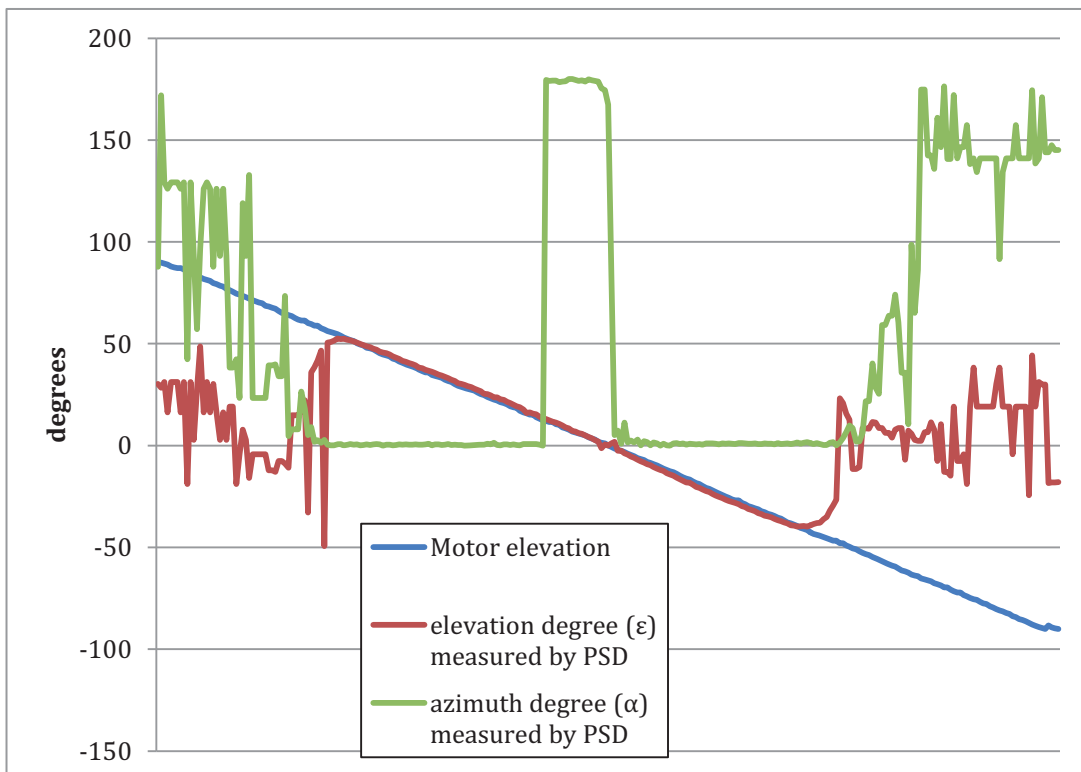ent setup. Each sequence part (see section 3.2) is programmed to run the elevation degree from -90° to +90° for all 7 azimuth positions from 0° to 90°. Since the light source is fixed, and the elevation motor turns around the new azimuth axis (solid line in figure 5-1) for every sequence part, the sensors are not able to recognize a change in azimuth degree. To avoid this problem, the motor has to be programmed to turn around its azimuth 0° axis (dashed line in figure 5-1) for every sensor azimuth position. While this determination problem is solved for satellites by using several sensors, which are mounted orthogonally, a single sensor can only determine two out of the pitch, roll and yaw angles.
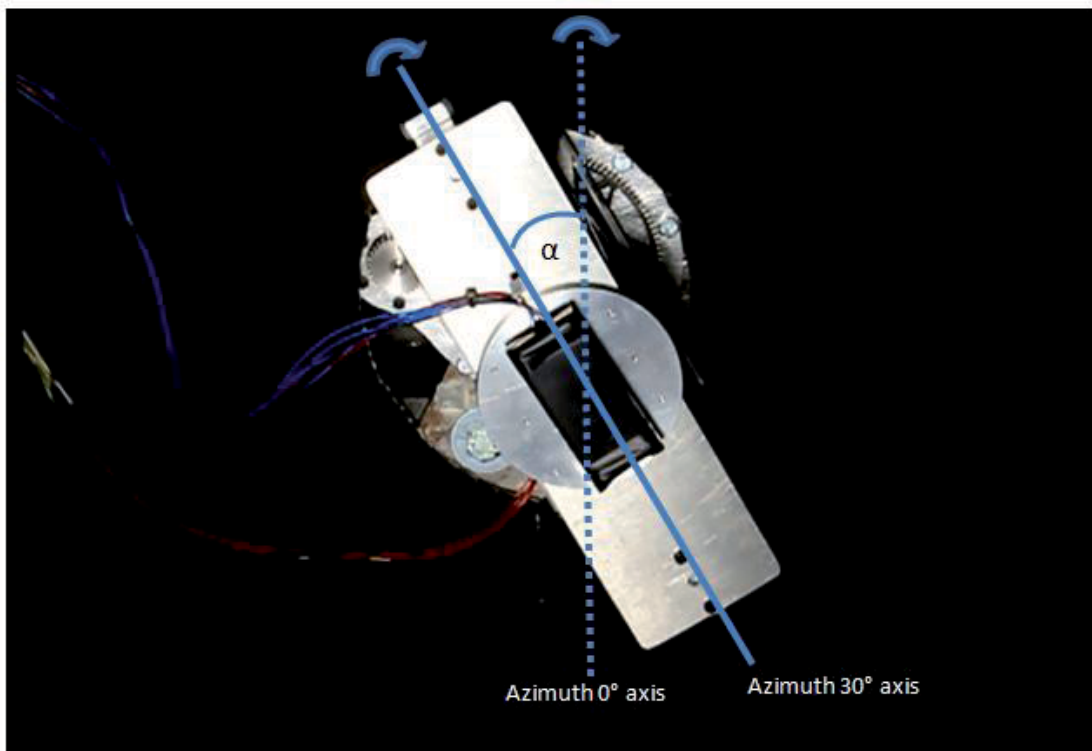

Figure 5–1: The LISA motor's faulty azimuth turning axis (solid line)

This flaw has only little impact on the Solar Cell 3G30C test results, because the cell can only determine the incidence angle in one dimension anyhow and therefore does not recognize a second angle change. Again, more angle determinations can be

achieved by the use of more cells, mounted in different positions. As a result, the cell's output data would not visibly change even if the motor sequence flaw was corrected.

The DTU sensor on the other hand, is, just like the PSD-based sensor, capable of determining two angle rotations. While both sensors precisely reflect the motor's elevation degree, the azimuth degree seems to stay the same during all 7 sequence parts. This means that, with this setup, the two sensors can only be directly compared in one angle determination – the elevation angle.

For the PSD-based sensor, predictions can be made on what it is expected to output for different azimuth degrees. Figures 5-2 and 5-3 show the calculated light spot positions on the PSD's active area within its FOV throughout two different motor sequence parts (0° and 45°). The light spot positions together form a straight line, which is tilted by as much as the sensor was tilted on its mount (due to mounting inaccuracies). On the active area the two axes are interchanged, so the y-axis runs horizontally. Because of the above stated sequence problem, both plots appear to be exactly the same. The plot that would be expected, if the problem was corrected is depicted by the dashed line (figure 5-3), which is rotated around point N (see section 3.6.1) by α (azimuth; in this case 45°) degrees. This prediction is based on the in section 3.6.1 introduced azimuth degree calculation. The azimuth graph of figure 4-9 has a constant value of about 0.6° (excluding the 180° maximum), which equals the sensor's measured mounting tilt. All in all, the motor sequence problem is only a minor drawback for the testing of the PSD-based sensor, because the Sun vector generation (section 2.2.2) accuracy is only directly affected by light spot and hole (in the aperture plate) position accuracy, which can be specified using the available test results that directly depend on the same two parameters.
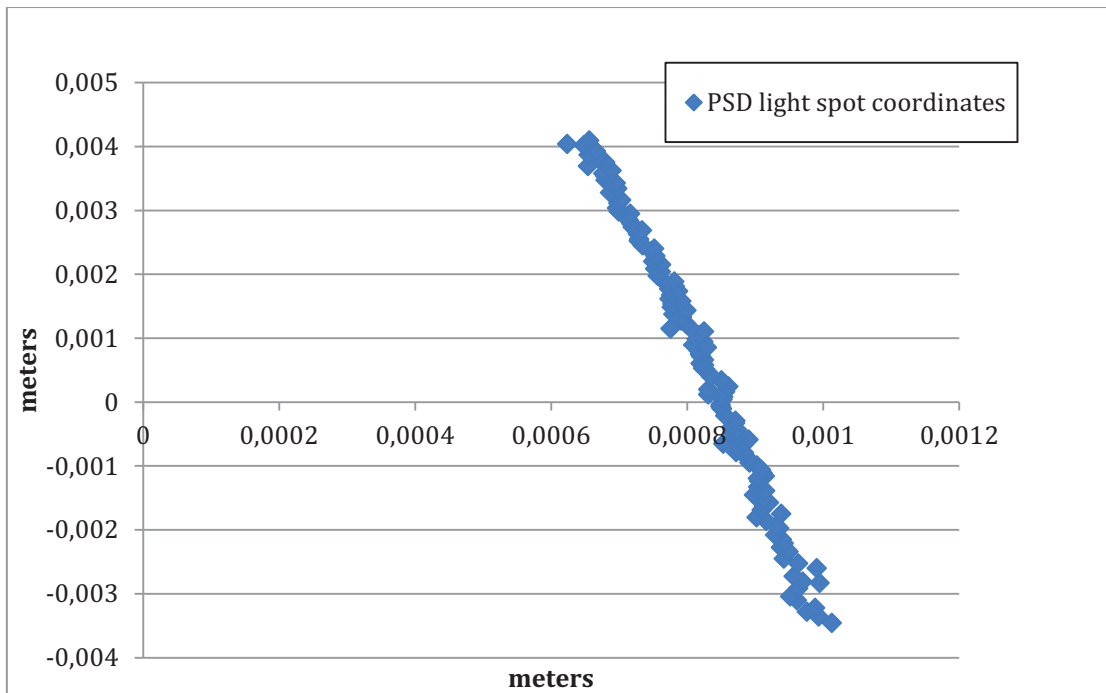
Figure 5–2: PSD light spot position plot for motor sequence part 1 (azimuth 0°)
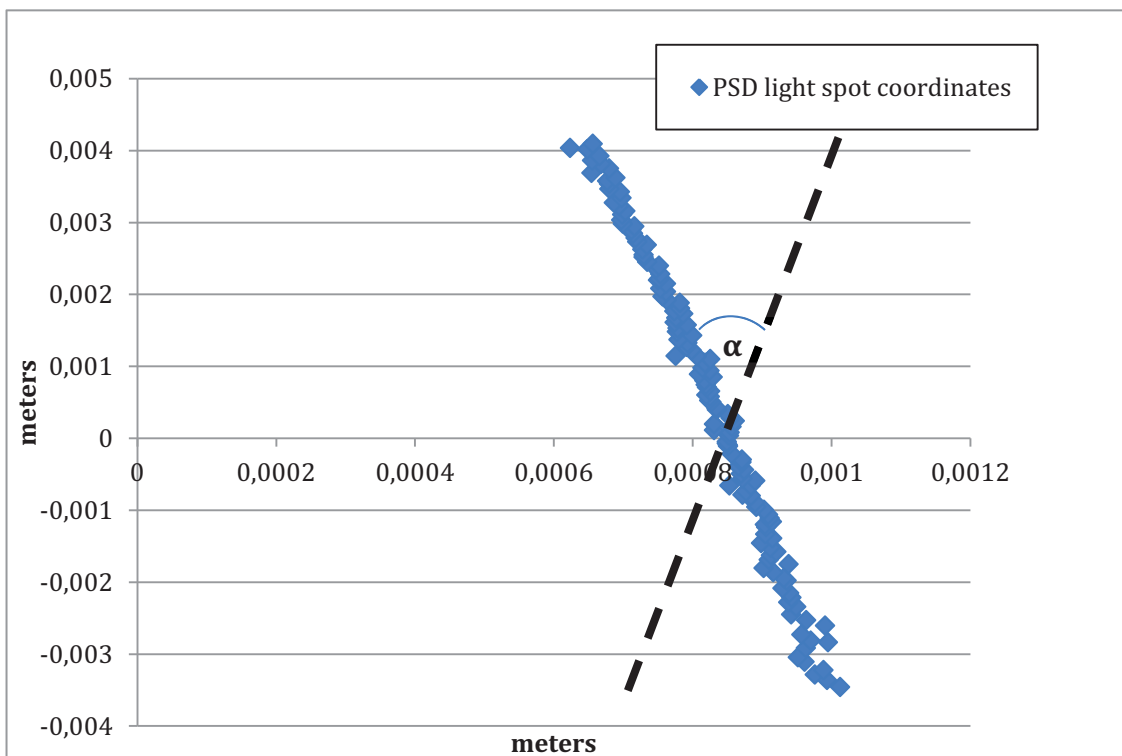

Figure 5–3: PSD light spot position plot for motor sequence part 4 (azimuth 45°) and expected coordinates (dashed line)

As stated before, the DTU sensor also outputs the same azimuth degree for all sequence steps. Figure 4-4 shows the plot of the calculated azimuth angle. The

average azimuth value is around 6°, which equals the slight tilt of the sensor mount (the values show that this sensor was tilted more than the PSD-based sensor). Despite the motor sequence drawback, the sensors can be compared in their elevation degree determination accuracy over 7 different alignment positions.

5.2 Performance Comparison of All Three Tested Sensors

The test results of section 4 render each sensor's measurement error in calculating the motor elevation degree for several azimuth positions. Since vector calculation is based on these angle measurements, the specified measurement error directly represents Sun vector generation accuracy. The more accurate a sensor determines the Sun vector, the better its attitude determination. For elevation degree determination the PSD-based Sun sensor performed best in accuracy with a measurement error of only 1.08° within a FOV of 90°, while it featured a more limited FOV (with the use of 5 mm spacers) than the other two tested systems, which is seen in figure 4-9. In this same FOV (90°) the DTU sensor achieved a measurement error 6.9°. Both its average experiment errors within the 90° and 140° FOV (8.5° error) are well above the specified accuracy of 1° within the 140° FOV. The reason for that is that the specified accuracy is the result of tests performed by Pedersen and Hales [18] at DTU with a different interface and circuit board. The interface and circuit board designed by Thomas Bickel (see section 1.3) therefore causes unforeseen inaccuracies for the sensor. This assumption is indicated by the noise of the sensor's output raw data seen in figure 4-3. Noise is also a vital problem for the tested solar cell. It did not deliver stable and reliable data that could have been used for attitude determination. Hence, the values of the trendline were used to calculate the incidence angle, which leaves the calculated accuracies for a FOV of 90° and 140° as estimates. This problem could be solved by attentively investigating the cell's circuit for error sources. Furthermore, the cell only allows for calculation of one orientation angle. Since there are only four cells mounted on different sides of the CubeSat, the overall constellation does not facilitate unambiguous attitude determination for the satellite. Another drawback regarding solar cell attitude determination is the fact that the cells are the satellite's experimental payload and have to be evaluated, where it is more reasonable to determine indispensable evaluation information for the cells externally.

The requirement of 1° accuracy (see section 2.1) is not entirely met by any of the tested systems. The PSD-based sensor is nevertheless very close with its 1.08° measurement error and therefore qualifies best as a suitable concept for attitude determination on MOVE.

Referring to section 2.1, the PSD-based sensor at this level fulfills nearly all requirements. The only parameters that still have to be evaluated for the smaller PSD version (S5990-01) are the expansion of the FOV to 140° (using smaller spacers), 1° accuracy, the sensor weight of 120 mg, and the thermal constraints (with the possible use of heaters).

5.3 Attitude Determination for MOVE Using the PSD-based Sun Sensor

5.3.1 Error Accumulation

It is impossible for any sensor to determine attitude with 100% accuracy. There are always error sources that have to be found and defined. The sum of all error sources is directly proportional to the measurement error of the sensor, which can be lowered as error sources are eliminated.

For the PSD-based sensor, error sources include PCB component inaccuracies, limited light spot resolution on the active area, as well as mounting and hardware construction inaccuracies. The voltage reference AD1582, mounted on the PCB, has a specified output tolerance of ±0.2 V [25], which increases the noisiness of the measurement. As observed in LabVIEW, the dimension-less output data of each channel has an inaccuracy of ±3. This includes the error sources created by the other components on the PCB. In addition, the PSD itself has a specified position detection error of ±150 μm [21]. Furthermore, the construction of the entire sensor unveils new possible error sources, of which the extent can hardly be measured. They include the distance between the active area and the aperture plate (h) and the hole size. Minor deflections of both dimensions have to be taken into account. Simultaneously, the hole size directly affects the intensity of light diffraction (although its scale is very small). An error parameter that cannot be eliminated, unless the hole size is variable, is the recommendation [21] of a spot light size larger than ø 0.2 mm 80% from the center of the active area to the edge, which entails minor inaccuracies, if not accounted for.

All these parameters in total are responsible for the sensor's measurement error of 1.08°.

5.3.2 The PSD-based Sensor's Functionality in Space

As already mentioned, a test setup never resembles the exact same environment as the sensor will encounter in space. For the PSD-based sensor a few test parameters change when the sensor is actually in orbit. One of those parameters is the sensor's zero degree position. While point N has coordinates N(x≠0 ; y≠0) due to mounting inaccuracies in the test setup, which limit light source alignment with the coordinate system's origin of the sensor, the aperture plate can be aligned with the active area to nearly output a value of 0 for both coordinates when the Sun is in the sensor's zenith position in space. (Note: limited construction accuracy will always cause a minor shift of point N from the PSD coordinate system's origin) With point N being nearly N(x=0 ; y=0) the sensor will have an evenly distributed FOV to all sides. Simultaneously this explains why the elevation degree measured by the PSD (figure 4-9) loses accuracy sooner when rotating in the negative elevation direction than when rotating in the other. There is simply less active area space on one side of point N than on the other. In the test setup this phenomenon entails a FOV of -40° to +50°. With proper alignment, a FOV of almost -45° to +45° (with the same spacers) could be reached in space.

As an alternative to the calculations of section 3.6.1, the satellites rotational angles can also be calculated using the known Sun vector. The vector obtained with formula (2-3) uses only light spot coordinates and the distance between the active area and the PSD (h), which define the real Sun vector in its own coordinate system. For the sensor in space, the two rotational angles that correlate with azimuth and elevation can be obtained from the Sun vector and the coordinate system's axes (see figure 5-4).

Another aspect that has to be kept in mind when finally integrating the sensor is the mathematical singularity of angle calculations. The consequence of this issue can be seen in figure 4-9, where the calculated azimuth degree at motor elevation positions around 0° has a value of 180° because the position is mathematically not clearly defined.
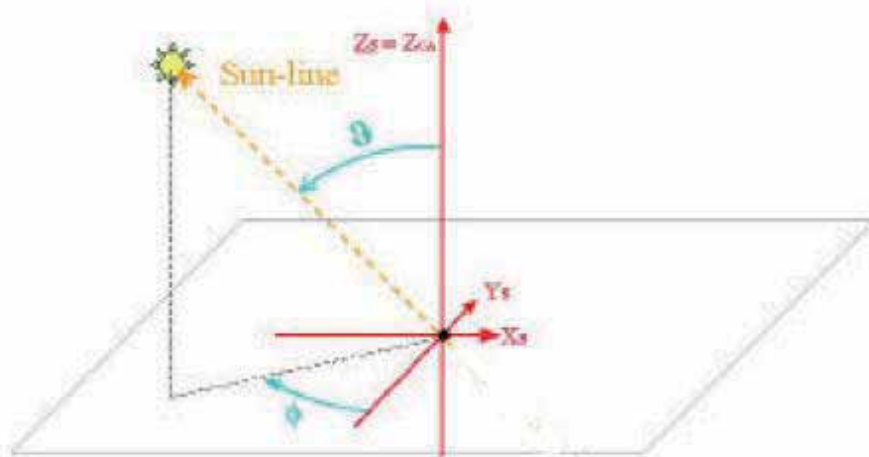
Figure 5–4: Correlating azimuth and elevation angles against the Sun vector

To finally be able to determine attitude for the satellite in all positions, several single sensors have to be mounted on different sides of the cube structure to cover the entire sphere around the spacecraft. MOVE currently hosts four Sun sensor mounts of 14 x 22 mm (designed for the DTU sensor). Only the sensors, which have the Sun in their current FOV will output the vector. This is handled via a filter system of the OBDH (on-board data handling) board. This filter system ideally extracts only usable data, which are obtained by the sensor within its specified FOV. Data that is usable but demands modification, like the above mentioned singularity issue, is also filtered and substituted for by this system. Exemplary, a look up table would assign the value of 0° for a calculated azimuth degree of 180°.

5.4 Sensor Integration Considerations for MOVE

As already mentioned, MOVE has four sensor mounts installed. They are all on the cube sides with the experimental payload so that whenever the payload is tested attitude information is available. Figure 5-5 shows the flight PCB layout of the top and bottom side as designed for the DTU sensor by Thomas Bickel [16].
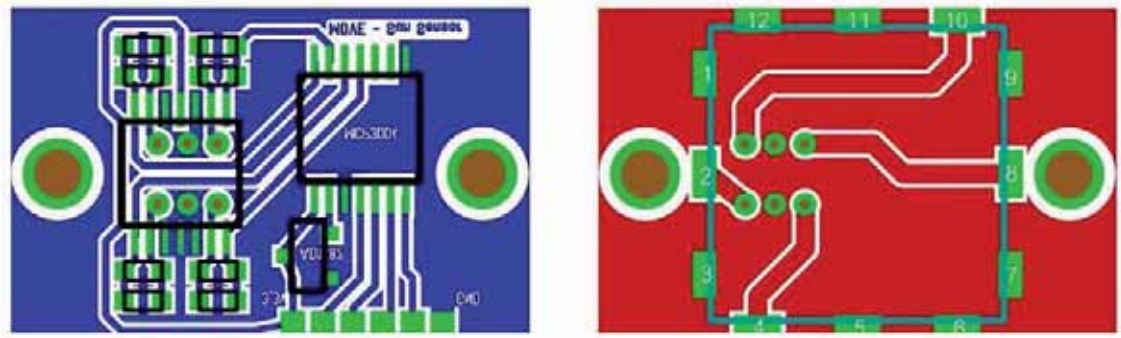
Figure 5–5: Top (right) and bottom (left) side of MOVE's Sun sensor flight PCB [16]

The bottom side shows the same PCB components as they are used on the PSD Sun sensor's test PCB (see figure 2-7). Therefore when integrating the small version of the PSD (S5990-01) on the top side only minor connection and layout changes have to be made. Finally, a suitable aperture plate that protects the PSD from undesired exposure to light has to be designed, while keeping in mind the total height constraint of 6 mm (see section 2.1). It is especially important to avoid backlighting of the circuit board. One of the mounted flight PCBs with the DTU sensors on MOVE are depicted in figure 5-6 (circled area).
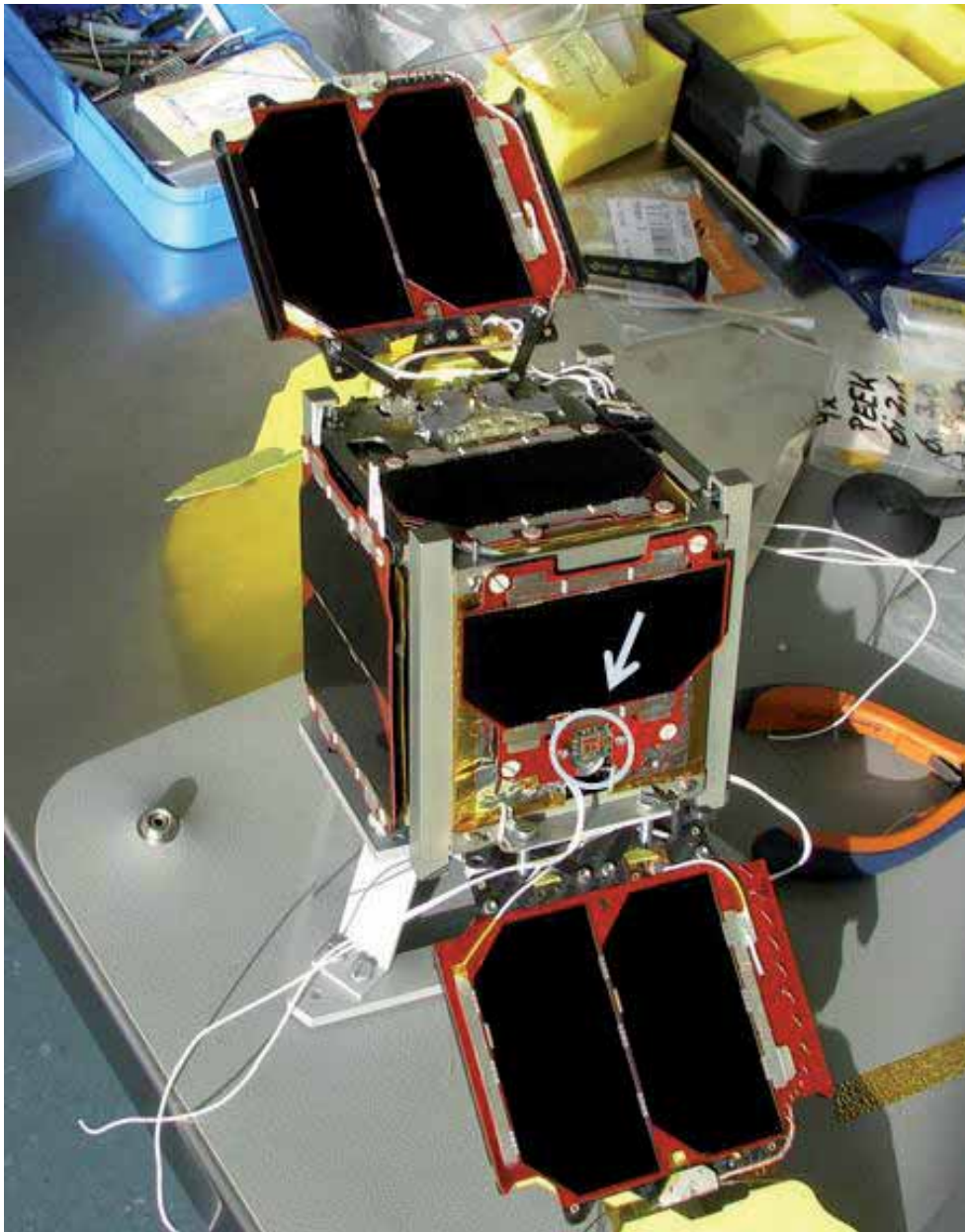
Figure 5–6: MOVE satellite with current PCB flight model for the DTU Sun sensor

The two extravehicular wings of the satellite limit the sensor's FOV due to shading. This aspect has to be kept in mind when determining attitude. A possible way to avoid problems caused by the wings is to identify satellite orientation positions where this phenomenon occurs and to discard the false attitude information when approaching the position.

All in all, the PSD-based sensor's concept fully supports the needs of the CubeSat and therefore has the potential of being integrated as a follow-up flight model.

5.5 Conclusion and Future Work

In this paper, the functionality of a new concept for attitude determination on the MOVE satellite was successfully developed and tested. However, the final design of a PSD-based sensor flight model exceeds the scope of this project. Follow-up projects are advised to focus on testing of the functionality of the small version of the PSD (S5990-01) and the expansion of the sensor's FOV. Other tasks to complete before final integration of the sensor include Sun vector transformation from each sensor's coordinate system to the body-fixed frame, thermal-vacuum testing the system, and an analysis of the impact of disruptive factors (like the Earth's albedo) on the sensor's output data.

Altogether this is just the first step toward complete attitude determination and only a small step toward a successful mission for MOVE, but if all small contributions piece together perfectly, the success of the mission is guaranteed.

A   Appendix

A.1   References

[1]   Claas Olthoff *MOVE overview. A First-MOVE in satellite development at TUM* (TUM Institute of Astronautics).

[2]   Dr. Mitch Bryson 2011 *Satellite Attitude Determination 1. AERO4701 Space Engineering 3.* lecture handouts for the Australian Centre for Field Robotics, University of Sydney. Available at http://www-personal.acfr.usyd.edu.au/m.bryson/Lectures/lecture_week7_handouts.pdf. Accessed: 12/01/11

[3]   Wiley J. Larson and James R. Wertz ed 2006 *Space Mission Analysis and Design. Third Edition* (Microcosm Press, CA and Springer, NY).

[4]   Wikipedia 2011 *Datum (geodesy).* Available at http://en.wikipedia.org/wiki/Datum_%28geodesy%29. Accessed: 12/01/11

[5]   Dr. Mitch Bryson 2011 *AERO4701: Space Engineering 3.* lecture handouts for the Australian Centre for Field Robotics, University of Sydney. Available at http://www-personal.acfr.usyd.edu.au/m.bryson/Lectures/lecture_week1_handouts.pdf. Accessed: 12/01/11

[6]   Wikipedia 2011 *Nadir.* Available at http://en.wikipedia.org/wiki/Nadir. Accessed: 12/02/11

[7]   Michael D. Griffin and James R. French 2004 *Space Vehicle Design* (American Institute of Aeronautics and Astronautics, Inc.).

[8]   NASA 2011 *NASA's Gravity Probe B Confirms Two Einstein Space-Time Theories. NASA's Latest News.* Available at http://www.nasa.gov/mission_pages/gpb/gpb_003.html. Accessed: 12/02/11

[9]   Texas Instruments *Accelerometeres and How they Work.* Available at http://www2.usfirst.org/2005comp/Manuals/Acceler1.pdf. Accessed: 12/07/11

[10] Wikipedia 2011 *Talk: South Pole.* Available at http://en.wikipedia.org/wiki/Talk%3ASouth_Pole. Accessed: 12/04/11

[11] NASA 1970 *Spacecraft Sun Sensors.* Available at http://www.dept.aoe.vt.edu/~cdhall/courses/aoe4065/NASADesignSPs/sp8047.pdf. Accessed: 12/03/11

[12] NASA 1969 *Spacecraft Earth Horizon Sensors.* Available at http://ntrs.nasa.gov/archive/nasa/casi.ntrs.nasa.gov/19700026254_1970026254.pdf. Accessed: 12/01/11

[13] Ball Aerospace and Technologies Corp. *Star Trackers.* Available at http://www.ballaerospace.com/page.jsp?page=104. Accessed: 12/07/11

[14] Ming Wang *Passive Magnetic Attitude Stabilization*.

[15] Nick Sweet 2011 *Hysteresis in Plain English. Attitude Control System.* Available at http://spaceconcordia.ca/2011/10/hysteresis-in-plain-english/. Accessed: 12/14/11

[16] Thomas Bickel 2009 *Electrical Design and Integration of Sun Sensors for the Picosatellite MOVE*.

[17] AZUR SPACE 2009 *30% Triple Junction GaAs Solar Cell. Type: TJ Solar Cell 3G30C.*

[18]   Martin Pedersen and Jan Hales 2004 *Linear Two-Axis MOEMS Sun Sensor. Part of the DTUsat project - and beyond.* Available at http://hvig.dk/files/Pedersen-and-Hales-2004-Linear-Two-Axis-MOEMS-Sun-Sensor-Technical-Report.pdf. Accessed: 12/17/11

[19]   ISIS - Innovative Solutions In Space *Miniaturised Analog Fine Sun Sensor.* Available at http://www.isispace.nl/brochures/ISIS_MINI_FSS_Brochures_v.7.11.pdf. Accessed: 12/17/11

[20]   Holger Adomat 2010 *Grundlagen einer PVAnlage / Sonnenenergie.* Available at http://www.nibis.ni.schule.de/~ruzbbsof/PDF%20Formate/Infoblatt%202.pdf. Accessed: 12/18/11

[21]   Hamamatsu Photonics K.K. S S D 2007 *Two-dimensional PSD S5990-01, S5991-01. Improved tetra-lateral type for surface mounting.*

[22]   EU-Kooperationsbüro Bayern Innovativ GmbH 2011 *Time-saving Printed Circuit Board Production Technology.* Available at http://www.technologiepartner.de/index.php?file=bbs-show.php&bbsref=11%20TR%2099PB%203KQD&PHPSESSID=k16ciap6jjb5939e ibluunup61. Accessed: 01/07/12

[23]   Analog Devices *Zero-Drift, Single-Supply, Rail-to-Rail Input/Output Operational Amplifiers. AD8551/AD8552/AD8554.* Available at http://www.analog.com/static/imported-files/data_sheets/AD8551_8552_8554.pdf. Accessed: 12/23/11

[24]   Wikipedia 2011 *Transimpedanzverstärker.* Available at http://de.wikipedia.org/wiki/Transimpedanzverst%C3%A4rker. Accessed: 01/05/12

[25]   Analog Devices *2.5 V to 5.0 V Micropower, Precision Series Mode Voltage References. AD1582/AD1583/AD1584/AD1585.* Available at http://www.analog.com/static/imported-files/data_sheets/AD1582_1583_1584_1585.pdf. Accessed: 12/23/11

[26]   Microchip Technology Inc. 2008 *MCP3004/3008. 2.7 V 4-Channel/8-Channel 10-Bit A/D Converters with SPI Serial Interface.* Available at http://ww1.microchip.com/downloads/en/DeviceDoc/21295C.pdf. Accessed: 12/23/11

[27]   Dr. David P. Stern 2004 *Coordinates. Azimuth and Elevation.* Available at http://www-istp.gsfc.nasa.gov/stargaze/Scelcoor.htm. Accessed: 12/23/11

[28]   NASA 2011 *Climate & Radiation. Solar Radiation.* Available at http://atmospheres.gsfc.nasa.gov/climate/index.php?section=136. Accessed: 12/14/11

[29]   Jordan Butler *The Sun: Light and Color Temperature.* Available at http://www.sewanee.edu/chem/Chem&Art/Detail_Pages/ColorProjects_2004/Butler/Butler.html. Accessed: 12/26/11

[30]   Universität zu Köln *Fehlerrechnung.* Available at http://www.ph2.uni-koeln.de/fileadmin/Lehre/Anfaengerpraktikum/Fehler.pdf. Accessed: 01/04/12

A.2   PSD PCB Connection Diagram
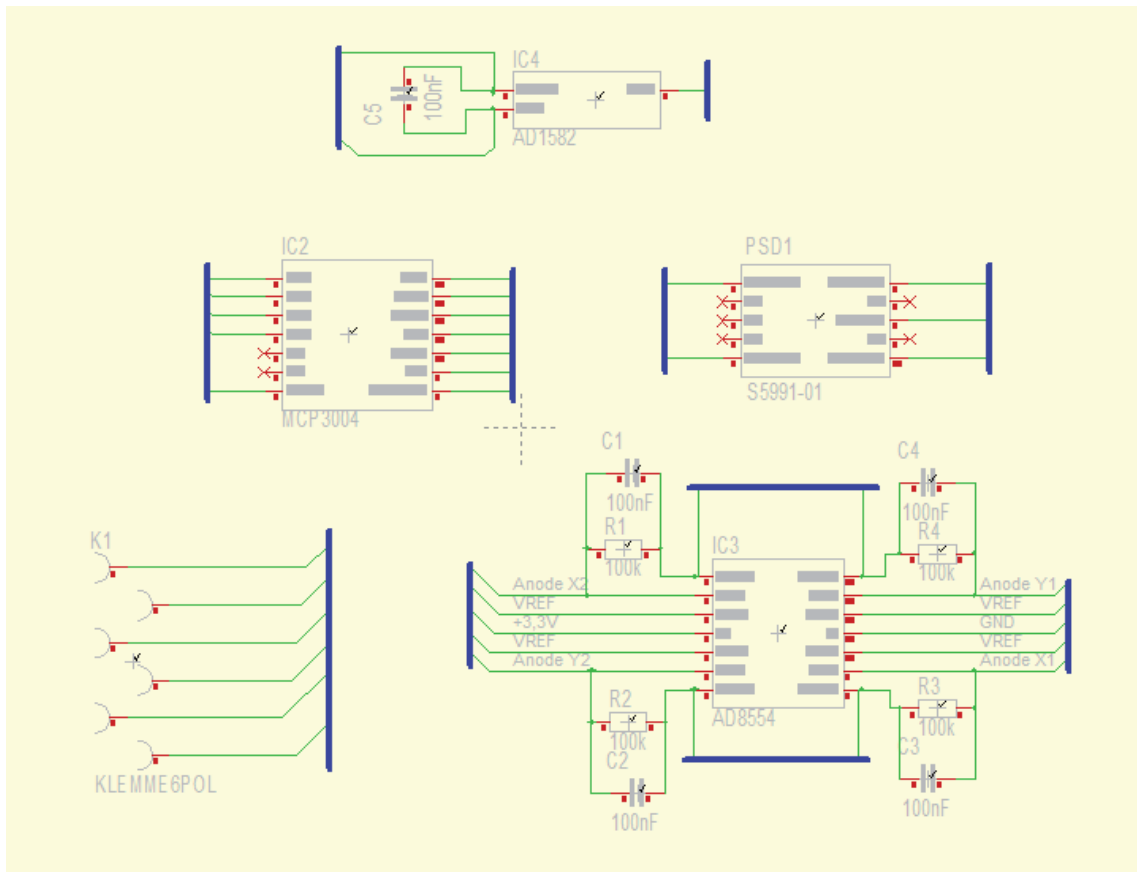
Appendix to section 2.3.2:

Figure A-1: TARGET connection diagram for the PSD test-PCB

A.3   LabVIEW Experiment Control VI
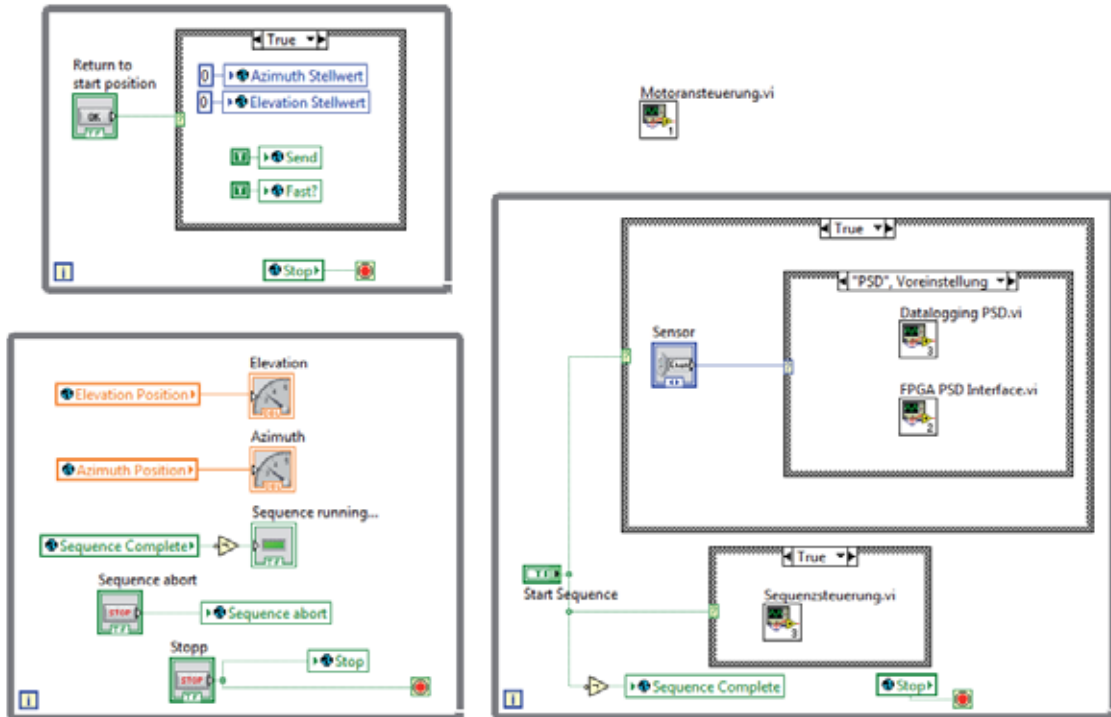
Appendix to section 3.5:

Figure A-2: LabVIEW block diagram for the experiment control VI

A.4   MATLAB Implementation of the PSD-based Sensor's Evaluation

The following MATLAB code is an appendix to section 3.7.1. The calculation of the azimuth degree is based on point N (x=0 ; y=0) and the elevation degree calculation yields absolute values only. To obtain positive and negative angle values the if-condition of section 3.7.1 has to be added.

```matlab
%commas (,) have to be replaced with dots (.) in text files before
loading them
%change axis scaling and varible z if motor turns slower/faster

clear; close all;

k=15; %constant for calculation of the azimuth position
j=2.5/1023; %j= single volt steps

for d=0:6

    o=k*d;  %variable for plot name

    if d==0
        m=load('0_Deg.txt');
    end
    if d==1
        m=load('15_Deg.txt');
    end
    if d==2
        m=load('30_Deg.txt');
    end
    if d==3
        m=load('45_Deg.txt');
    end
    if d==4
        m=load('60_Deg.txt');
    end
    if d==5
        m=load('75_Deg.txt');
    end
    if d==6
        m=load('90_Deg.txt');
    end
```

```matlab
for z=1:270

realElevation=m(z,3);

    %calculation of azimuth and elevation angle measured by the PSD

kVoltAmplifier1 = m(z,4) * j;
kVoltAmplifier1Var = 2.5 - kVoltAmplifier1;
kCurrentAnodeY1 = kVoltAmplifier1Var / 680000;


kVoltAmplifier2 = m(z,5) * j;
kVoltAmplifier2Var = 2.5 - kVoltAmplifier2;
kCurrentAnodeX1 = kVoltAmplifier2Var / 680000;


kVoltAmplifier3 = m(z,6) * j;
kVoltAmplifier3Var = 2.5 - kVoltAmplifier3;
kCurrentAnodeY2 = kVoltAmplifier3Var / 680000;


kVoltAmplifier4 = m(z,7) * j;
kVoltAmplifier4Var = 2.5 - kVoltAmplifier4;
kCurrentAnodeX2 = kVoltAmplifier4Var / 680000;


kVar1 = kCurrentAnodeX2 + kCurrentAnodeY1;
kVar2 = kCurrentAnodeX1 + kCurrentAnodeY2;
kVar3 = kVar1 - kVar2;
kVar4  =  kCurrentAnodeX1  +  kCurrentAnodeX2  +  kCurrentAnodeY1  +
kCurrentAnodeY2;
kVar5 = kVar3 / kVar4;
kVar6 = kVar5 * 0.01; %size of PSD active area: 0.01 by 0.01 meters
kPosX = kVar6 / 2;


kVarr1 = kCurrentAnodeX2 + kCurrentAnodeY2;
kVarr2 = kCurrentAnodeX1 + kCurrentAnodeY1;
kVarr3 = kVarr1 - kVarr2;
kVarr5 = kVarr3 / kVar4;
kVarr6 = kVarr5 * 0.01;
kPosY = kVarr6 / 2;


    %conversion of x and y position of the light spot into measured
(by
    %PSD)elevation and azimuth degree:

PN=sqrt((kPosX-6.0241*10^-5)^2+(kPosY-6.0241*10^-5)^2);     %distance
between PSD light point and PSD reference (center) light point
```

```matlab
a=kPosY;
b=kPosX;
p=(a^2)+(b^2);


f=sqrt(p);


R=f/0.00374; %height between PSD and aperture plate: 3.74mm
R=PN/0.00374; %height between PSD and aperture plate
T=a/b;


M=atan(R);    %E=absolute elevation degree measured; arctangent for
inverse                   trigonometry
N=atan(T);    %A=azimuth degree measured; arctangent for inverse
trigonometry
E=radtodeg(M); %conversion of radians to degrees
A=radtodeg(N);


if z==1
    figure  %create figure on first loop count
end


plot(z, A, 'g.');
xlabel('measurment N°');
ylabel('degree');
number=num2str(o);
title(char({'azimuth  (green)  and  elevation  (pink)  degree'  'azimuth
degree' number}));
axis([0 300 -90 +90]);  %scale of x and y axis
grid on
hold on;


plot(z, E, 'm.');


plot(z, realElevation, 'b.');


if z==270
hold off;
end


end
end
```